arXiv:astro-ph/0607551v2 17 Jan 2007

A MULTI-WAVELENGTH STUDY OF 1WGA J1346.5−6255: A NEW γ CAS ANALOG UNRELATED TO THE BACKGROUND SUPERNOVA REMNANT G309.2−00.6

Samar Safi-Harb[1,2], Marc Ribó[3,4], Yousaf Butt[5], Heather Matheson[1], Ignacio Negueruela[6], Fangjun Lu[7], Shumei Jia[7], Yong Chen[7]

To appear in the Astrophysical Journal, v659n1, April 2007

ABSTRACT

1WGA J1346.5−6255 is a *ROSAT* X-ray source found within the radio lobes of the supernova remnant (SNR) G309.2−00.6. This source also appears to coincide with the bright and early-type star HD 119682, which is in the middle of the galactic open cluster NGC 5281. The radio morphology of the remnant, consisting of two brightened and distorted arcs of emission on opposite sides of the 1WGA J1346.5−6255 source and of a jet-like feature and break in the shell, led to the suggestion that 1WGA J1346.5−6255/G309.2−00.6 is a young analog of the microquasar SS 433 powering the W50 nebula. This motivated us to study this source at X-ray and optical wavelengths. We here present new *Chandra* observations of 1WGA J1346.5−6255, archival *XMM-Newton* observations of G309.2−00.6, and optical spectroscopic observations of HD 119682, in order to search for X-ray jets from 1WGA J1346.5−6255, study its association with the SNR, and test for whether HD 119682 represents its optical counterpart. We do not find evidence for jets from 1WGA J1346.5−6255 down to an unabsorbed flux of 2.6×10^{-13} ergs cm^{-2} s (0.5–7.5 keV), we rule out its association with G309.2−00.6, and we confirm that HD 119682 is its optical counterpart. We derive a distance of 1.2 ± 0.3 kpc, which is consistent with the distance estimate to NGC 5281 (1.3 ± 0.3 kpc), and much smaller than the distance derived to the SNR G309.2−00.6. We discuss the nature of the source, unveil that HD 119682 is a Be star and suggest it is a new member of the recently proposed group of γ-Cas analogs. The *Chandra* and *XMM-Newton* X-ray lightcurves show variability on timescales of hundreds of seconds, and the presence of a possible period of ∼1500 s that could be the rotational period of an accreting neutron star or white dwarf in this γ-Cas analog.

Subject headings: X-rays: individual: 1WGA J1346.5−6255, 1RXS J134633.6−625528, SNR G309.2−00.6 – stars: individual: HD 119682 – stars: emission-line, Be – open clusters and associations: individual: NGC 5281 – ISM: individual: G309.2−00.6 – ISM: abundances –

1. INTRODUCTION

X-ray observations of Supernova Remnants (SNRs) have been continuously shaping our understanding of the diversity of compact objects associated with them. While the Crab used to be the prototype example for the aftermath of a supernova explosion, there is now growing evidence for a diversity of compact objects associated with SNRs. These include the magnetically powered neutron stars or magnetars, the radio-quiet neutron stars, the high-magnetic field radio pulsars, and accretion-powered candidates. Out of the 236 catalogued Galactic SNRs however, W50/SS 433 remains the only system confirmed to harbor a microquasar (a neutron star or black hole in a binary system emitting a two-sided semi-relativistic jet). The search for other such systems is needed not only to address the uniqueness of W50/SS 433, but also to study the connection between supernovae and microquasars.

To date, there are just six confirmed microquasars with massive optical companions in our Galaxy (Paredes 2005). Since the physics of the accretion-ejection phenomenon in microquasars (and AGN) central engines is not well understood, each additional SNR-microquasar system helps greatly to constrain the theoretical models. Here we present a study of the G309.2−00.6/1WGA J1346.5−6255 system which has been proposed to be a young analog of the W50/SS 433 system.

1.1. *G309.2−00.6 and 1WGA J1346.5−6255*

G309.2−00.6 was first identified as an SNR based on its nonthermal radio emission (Green 1974). A detailed study of the SNR was performed using the Australia Telescope Compact Array (ATCA, Gaensler et al. 1998). The remnant has a distorted shell-like morphology (see Fig. 1 and Fig. 2) with two brightened and distorted arcs of emission on opposite sides with diameters of 12′ and 15′, a jet-like feature and breaks in the shell. The SNR has a surface brightness of 5.4×10^{-21} W m^{-2} Hz^{-1} Sr^{-1} at 0.843 GHz (Whiteoak & Green 1996). Interestingly, this morphology resembles almost exactly a scaled down version of the SNR W50 (see, e.g., Dubner et al. 1998), well known to be powered by the microquasar SS 433. H I absorption measurements against the SNR yield a distance in the range 5.4–14.1 kpc, corresponding to an age of $(1-20)\times10^3$ yr (Gaensler et al. 1998).

Infrared observations of the remnant show no obvious emission from G309.2−00.6 (Gaensler et al. 1998), but strong emission coincident with the nearby object RCW 80, identified as an H II region based on its infrared and Hα emission

[1] Department of Physics and Astronomy, University of Manitoba, Winnipeg, MB, R3T 2N2, Canada; safiharb@cc.umanitoba.ca

[2] Department of Physics, George Washington University, 725 21st Street NW, Washington, DC 20052

[3] Departament d'Astronomia i Meteorologia, Universitat de Barcelona, Martí i Franquès 1, 08028 Barcelona, Spain

[4] AIM - Astrophysique Interactions Multi-échelles (UMR 7158 CEA/CNRS/Université Paris 7 Denis Diderot), CEA Saclay, DSM/DAPNIA/Service d'Astrophysique, Bât. 709, L'Orme des Merisiers, 91191 Gif-sur-Yvette Cedex, France

[5] Harvard-Smithsonian Center for Astrophysics, 60 Garden St., Cambridge, MA 02138, USA

[6] Departamento de Física, Ingeniería de Sistemas y Teoría de la Señal, Escuela Politécnica Superior, Universitat d'Alacant, Ap. 99, 03080 Alicante, Spain

[7] Key Laboratory of Particle Astrophysics, Istitute of High Energy Physics, Chinese Academy of Sciences, Beijing 100049, P.R., China

and flat radio spectrum. H I absorption measurements indicate a distance of 5.4±1.6 kpc towards RCW 80. Gaensler et al. (1998) suggest that the SNR may be interacting with the adjacent H II region, which would put the SNR at the lower range of the suggested distance and would imply an age ≤4,000 years. The striking resemblance of the radio morphology of G309.2−00.6 to W50 and the radio jet feature which aligns with the axis of symmetry defined by the two ears led Gaensler et al. (1998) to suggest that the SNR is powered by a central source producing collimated outflows, or jets, in two opposed directions, like the microquasar SS 433. A central source, however, has not been detected in the radio band, with a 5σ upper limit of 0.4 mJy at 1.3 GHz.

X-ray observations of G309.2−00.6 with the Advanced Satellite for Cosmology and Astrophysics (*ASCA*) have shown that the SNR is rich in thermal emission from a metal-rich ejecta-dominated plasma (Rakowski et al. 2001), indicating a young SNR age (700–4,000 years old). The X-ray spectrum of the SNR is best fitted with a non-equilibrium ionization model with a column density $N_{\rm H} \sim 0.6 \pm 0.3 \times 10^{22}$ cm^{-2}, yielding an estimated distance of 4±2 kpc to the remnant.

A bright *ROSAT* X-ray point-like source, 1RXS J134633.6−625528 also known as 1WGA J1346.5−6255 (White et al. 1996), with a count rate of 0.06±0.02 counts s^{-1} is located near the center of the radio emission from the SNR. This source is coincident with the early-type star HD 119682, the third brightest star in the middle of the galactic open cluster NGC 5281 (see §1.2). Rakowski et al. (2001) suggested the possibility that this source is related to the SNR based on its position and derived column density of $(0.3–1.0)\times 10^{22}$ cm^{-2}.

1.2. *HD 119682*

The star HD 119682 has been usually classified as one of the members of NGC 5281. Although it has been observed several times (see available V and $B-V$ photometry in Table 1) no precise spectral type and luminosity class have ever been reported, preventing an accurate estimation of the distance to this star. HD 119682 was initially classified as having a B spectral type by Cannon & Pickering (1918), and later on Stephenson & Sanduleak (1971) gave an OB+ spectral type. Moffat & Vogt (1973) suggest a luminosity class of III? and quote a distance of 1.30 kpc to NGC 5281 based on its unevolved stars. These authors also note that star #3, HD 119682, has an unusual position in the color-color diagram (CCD) and color-magnitude diagram (CMD). Humphreys (1975) reports a Be spectral type, while Fitzgerald et al. (1979) give a slightly different spectral type of O9e, although no luminosity class is specified. Based on the position of HD 119682 in the CCD and CMDs by Moffat & Vogt (1973), Mermilliod (1982) classified the object as a blue straggler.

A detailed study of NGC 5281 was carried out by Sanner et al. (2001). They report further photometry for HD 119682 and explicitly state that they do not see evidence for a blue straggler nature in the CMDs when compared to other stars of NGC 5281. Based on isochrone fitting to the CMDs of the cluster members they provide the following parameters: $(m-M)_0 = 11.0 \pm 0.2$ mag, $d = 1580 \pm 150$ pc, $E_{B-V} = 0.20 \pm 0.02$ mag, an age of $t = 45 \pm 10$ Myr (or $\log t({\rm yr}) = 7.65 \pm 0.10$) and a solar metallicity of $Z = 0.02$.

Levenhagen & Leister (2004) report the following physical parameters by fitting the spectral profile of HD 119682 with a non-LTE model: $v \sin i = 220 \pm 20$ km s^{-1}, $T_{\rm eff} = 31910 \pm$

550 K (or $\log T_{\rm eff}({\rm K}) = 4.504 \pm 0.008$), $\log g = 4.00 \pm 0.10$ dex, $\log t({\rm yr}) = 6.60 \pm 0.10$ (or $t = 4 \pm 1$ Myr), $\log L/L_\odot = 4.64 \pm 0.10$ and $M = 18 \pm 1\ M_\odot$. Note that the derived age is an order of magnitude smaller than the one of NGC 5281 reported by Sanner et al. (2001), clearly reinforcing the blue straggler nature of the star.

Finally, we note that near infrared photometry of HD 119682 is present in the 2MASS catalog: $J = 7.350 \pm 0.027$, $H = 7.184 \pm 0.033$, and $K_s = 6.950 \pm 0.023$ mag (Cutri et al. 2003; Skrutskie et al. 2006).

The goal of this paper is to study the nature of the 1WGA J1346.5−6255 source, its association with the optical star HD 119682, and the association of either source with the SNR G309.2−00.6. The previous proposal that G309.2−00.6 represents a young analog of W50 motivated us to study the *ROSAT* X-ray source and any associated jets with the *Chandra* X-ray Observatory. We also complement our X-ray study with archival observations obtained with *XMM-Newton*. While a detailed study of the diffuse emission from the SNR is beyond the scope of the paper, we here focus on the possible association between the X-ray source and the SNR. We also present new optical observations of HD 11968 acquired with ESO's New Technology Telescope. These observations are targeted to pin down the spectral type and luminosity class of the star from which to obtain a good estimate of its distance.

The paper is organized as follows. In §2, we summarize the observations undertaken at X-ray and optical wavelengths. In §3, 4, and 5, we present our *Chandra*, *XMM-Newton*, and the optical results, respectively. We finally discuss our results in §6 and summarize our conclusions in §7.

2. OBSERVATIONS AND DATA REDUCTION

The *ROSAT* source 1WGA J1346.5−6255 was observed with the *Chandra* X-Ray Observatory for 15.12 ks on 2004 December 26, with the back-illuminated chip S3 of the Advanced CCD Imaging Spectrometer (ACIS-S; G. Garmire[8]), at a focal plane temperature of −120 °C [9]. The data was processed using the standard CIAO 3.2.1 tools[10]. Events with ASCA grades (0, 2, 3, 4, 6) were retained, and periods of high-background rates were removed. The net effective exposure time was 14.9 ks. The data was corrected for Charge Transfer Inefficiency (CTI) using the Penn State corrector (Townsley et al. 2002) and filtered using the filtering available in acis_process_events (CIAO 3.2.1 with CALDB version 3.0.1).

The 1WGA J1346.5−6255 source spectrum was created by selecting photons within a circle of radius 3″.5 and centered at the peak of the X-ray emission (see §3.1). The background was selected from an annulus centered on the X-ray source, with inner radius of 10″ and outer radius of 15″. The count rate for the source was 0.104 ± 0.005 counts sec^{-1} and the count rate for the background was 0.004 ± 0.002 counts sec^{-1}. The spectrum was grouped to a minimum of 20 counts per bin and the energy range selected for spectral fitting was 0.5–7.5 keV (the spectrum is background dominated above 7.5 keV). The spectral analysis was performed using XSPEC version 11.2 [11].

The SNR G309.2−00.6 was observed by the European Photon Imaging Camera (EPIC) aboard *XMM-Newton*

---

[8] See http://cxc.harvard.edu/proposer/POG
[9] For a review of *Chandra*, see http://cxc.harvard.edu/cdo/about_chandra/overview_cxo.htm
[10] http://cxc.harvard.edu/ciao
[11] http://xspec.gsfc.nasa.gov

(Jansen et al. 2001) for 40.6 ks on 2001 August 28 (obs ID 0087940201). The EPIC-PN camera was operating in Extended Full Frame mode, and the EPIC-MOS cameras in Full Frame mode. A thick filter was used to avoid problems with bright stars in the open cluster NGC 5281. The data were processed using version 6.0 of the *XMM-Newton* Science Analysis Software (SAS). We created filtered event files using the EPIC-PN and MOS cameras in the 0.3–10 keV energy range. We then selected events for which the pattern was less than or equal to 4 (12) for PN (MOS), we removed the bad pixels, and cleaned the data by removing the times with high background proton flares. The resulting effective exposure time is 23.9 ks for PN, 27.8 ks for MOS1, and 27 ks for MOS2. The spectrum for 1WGA J1346.5−6255 was extracted using a circle centered at the peak of X-ray emission: $\alpha = 13^{\rm h}\ 46^{\rm m}\ 32\overset{\rm s}{.}6$, $\delta = -62°\ 55'\ 27''$ (J2000) and with a $0\overset{'}{.}5$ radius. The spectrum of the diffuse emission from G309.2−00.6 was extracted using a circle centered at the peak of the diffuse X-ray emission: $\alpha = 13^{\rm h}\ 46^{\rm m}\ 33^{\rm s}$, $\delta = -62°\ 50'\ 57''$ (J2000) and a radius of $3\overset{'}{.}125$. This region is shown in Fig. 2. The background spectrum for 1WGA J1346.5−6255 was extracted from a ring centered at the source and extending from $0\overset{'}{.}5$ to $1\overset{'}{.}0$; while the background spectrum for the diffuse emission was extracted from an annulus centered at the diffuse emission and of $5\overset{'}{.}83$ and $9\overset{'}{.}17$ for the inner and outer radii, respectively. The ancillary and response matrix files were produced using the SAS commands *arfgen* and *rmfgen*, respectively. The spectra were subsequently grouped into a minimum of 50 counts per bin for the point source and 200 counts per bin for the diffuse emission. The spectral analysis was subsequently performed using XSPEC v11.2.

We observed HD 119682 using the ESO Multi-Mode Instrument (EMMI) on the 3.5-m New Technology Telescope (NTT) at La Silla, Chile, on 2003 June 5th. An Hα spectrum was taken with the red arm in intermediate-resolution mode (REMD) and grating #6. The red arm is equipped with a mosaic of two thin, back-illuminated 2048×4096 MIT/LL CCDs and this configuration results in a nominal dispersion of 0.4 Å pixel^{-1} over the range $\lambda\lambda$ 6440–7150 Å. The resolution, measured on arc lines, is ≈ 1.2 Å. The blue spectrum was taken with the blue arm in intermediate-resolution mode (BLMD) and grating #12. The blue arm is equipped with a Textronik TK1034 thinned, back-illuminated 1024×1024 CCD and this configuration results in a nominal dispersion of 0.9 Å pixel^{-1} over the range $\lambda\lambda$ 3820–4750 Å. The resolution, measured on arc lines, is ≈ 2.6 Å. Image pre-processing was carried out with *MIDAS* software, while data reduction was achieved with the *Starlink* packages CCDPACK (Draper et al. 2000) and FIGARO (Shortridge et al. 1997).

3. *CHANDRA* RESULTS

3.1. *Imaging*

In Fig. 1, we show the radio image of the SNR G309.2−00.6 obtained with the Molonglo Observatory Synthesis Telescope (MOST) at a frequency of 0.843 GHz overlayed with the X-ray emission detected in the S3 chip of *Chandra*. The peak of the X-ray emission is located at $\alpha = 13^{\rm h}\ 46^{\rm m}\ 32\overset{\rm s}{.}6$, $\delta = -62°\ 55'\ 24''$ (J2000) with an error radius of $1\overset{''}{.}3$ (90% confidence level). This source corresponds to the previously known *ROSAT* source 1WGA J1346.5−6255.

Our primary goal is to search for any jets associated with this X-ray source. Since jets from compact objects generally peak at different X-ray energies than their powering en-

gines, we created energy images for 1WGA J1346.5−6255 in the soft (0.3–1.3 keV), medium (1.3–2.2 keV), and hard (2.2–10 keV) band. The energy boundaries were chosen as to obtain a similar number of counts (∼500) in each image. The images were then smoothed using the CIAO tool *csmooth* with a circular Gaussian kernel and are shown in Fig. 3. The initial smoothing scale was 1 pixel. The smoothing scale was increased (to a maximum 2 pixels) until the number of counts under the kernel exceeded a signal-to-noise ratio of 2. Where the signal-to-noise ratio was less than 2, the image was smoothed on a scale of 2 pixels. The axis overlayed on top of the images, and running from northeast to southwest, delineates the axis of symmetry of the radio lobes of G309.2−00.6, ≃ 45° counter-clockwise from north (Gaensler et al. 1998). Interestingly, there is a hint of extension in the soft energy band along this axis. However, any extension observed in Fig. 3 (purple, dark blue) has a count rate of less than 0.7 counts pixel^{-1}, indicating that the apparent extension is most likely background noise.

In order to further determine whether 1WGA J1346.5−6255 is point-like or extended, we subsequently compared its spatial characteristics with *Chandra*'s point spread function (PSF). We generated a PSF image at an offset axis of $0\overset{'}{.}48$ (the location of the source on the S3 chip) and at an energy of 1.5 keV (characteristic of the source's energy histogram). We subsequently normalized the PSF image to the source counts (∼1450 counts in the 0.3–10 keV range) and used the PSF as a convolution kernel when fitting the source. Fitting a two-dimensional Gaussian distribution to the data, we found that the full width half maximum (FWHM) was only slightly larger than the FWHM of the PSF which is assumed to be circular ($1\overset{''}{.}02$ and $0\overset{''}{.}73$, respectively). The data and PSF are shown in Fig. 4. Since the difference is less than one pixel ($0\overset{''}{.}4920 \pm 0\overset{''}{.}0001$), the data is consistent with a point source. A similar profile was created for the soft (0.3–2.4 keV) and hard energy band (2.4–10 keV), by evaluating the PSF at 1.1 keV and 2.5 keV, respectively. The FWHM of the data and PSF in the soft band was found to be $0\overset{''}{.}97$ and $0\overset{''}{.}73$, respectively. For the hard energy band, the FWHM of the data and PSF was $1\overset{''}{.}09$ and $0\overset{''}{.}77$, respectively. We conclude that the data in either band are consistent with a point source, and therefore rule out the presence of jets associated with 1WGA J1346.5−6255, down to an unabsorbed flux of 2.6×10^{-13} ergs cm^{-2} s^{-1} in the 0.5–7.5 keV range (see next section).

3.2. *Spectroscopy*

In order to address the nature of 1WGA J1346.5−6255, we fitted its spectrum with thermal and non-thermal models, modified by interstellar absorption. In Table 2, we summarize the parameters of the best fit models. Errors are at the 90% confidence level throughout the paper, unless otherwise mentioned. We find that blackbody and thermal bremsstrahlung models do not provide acceptable fits. The absorbed power-law model provides an adequate fit with the following parameters: a column density $N_{\rm H} = 0.18^{+0.08}_{-0.07} \times 10^{22}$ cm^{-2}, a photon index $\Gamma = 1.4 \pm 0.2$ and an unabsorbed flux of $1.1^{+0.3}_{-0.2} \times 10^{-12}$ ergs cm^{-2} s^{-1} in the 0.5–7.5 keV range (reduced $\chi^2_\nu = 0.46$, $\nu = 61$ degrees of freedom). The spectrum and fitted model are shown in Fig. 5, while in Fig. 6 we show the 68, 95 and 99.7% confidence contours for $N_{\rm H}$ and Γ. By examining the residuals in Fig. 5, some line emission appears to exist around 1 keV. For this purpose, we added

a MEKAL component (which would, e.g., account for any emission associated with coronal emission from a normal star, see §6.5 for more details). We find that the fit improves significantly ($\chi_\nu^2 = 0.341$, $\nu = 59$), with an F-test probability of 4.5×10^{-5} that this improvement occurs by chance. This best fit model is shown in Fig. 7 and the parameters are: $N_H = 0.19^{+0.13}_{-0.08} \times 10^{22}$ cm^{-2}, $\Gamma = 1.24^{+0.28}_{-0.26}$, $kT = 0.97^{+0.37}_{-0.28}$ keV, with an unabsorbed flux in the 0.5–7.5 keV energy range of $1.18^{+0.35}_{-0.29} \times 10^{-12}$ ergs cm^{-2} s^{-1}, very similar to the one obtained with a pure absorbed power law.

In order to test whether the X-ray emission is coronal emission from a normal star (see §6.5), pure MEKAL models were attempted. A single temperature MEKAL model yields a statistically acceptable fit, however the temperature is high and unconstrained (see Table 2). A two-component MEKAL model yields as good a fit as the power-law+MEKAL model but with the temperature of the hard component poorly constrained: $N_H = 0.19^{+0.09}_{-0.07} \times 10^{22}$ cm^{-2}, $kT_1 = 0.95^{+0.34}_{-0.24}$ keV; $kT_2 = 80$ (≥ 14) keV, and a reduced $\chi_\nu^2 = 0.342$ for $\nu = 59$ degrees of freedom. The temperature of the hard component, of $\sim 9 \times 10^8$ K, is unrealistically high and poorly constrained– we show in the next section that the *XMM-Newton* data helps better constrain this component. We conclude that while the two-component MEKAL model and the power-law+MEKAL model both yield statistically acceptable fits, the *Chandra* spectrum is best fitted and its parameters better constrained using the power-law+MEKAL model.

In order to quantify the upper limit on the flux from any unseen jets associated with 1WGA J1346.5−6255, we added a power-law component to the best fit power-law+MEKAL model above. We then froze the parameters of the model for 1WGA J1346.5−6255 and allow the photon index for any 'unseen' jets to vary between 1.6–2.0, which is reasonable based on observations of other jet sources. We find that the corresponding upper limit on the unabsorbed flux is 2.6×10^{-13} ergs cm^{-2} s^{-1} in the 0.5–7.5 keV range. At a distance of 1.3 kpc (see §6), this translates to a luminosity of $\sim 5.3 \times 10^{31}$ ergs s^{-1}.

3.3. *Timing*

To check for variability of 1WGA J1346.5−6255, we created lightcurves with *Chandra* data binned at 100, 120 and 150 s time intervals. The obtained lightcurves display variability with an amplitude at the $\pm 30\%$ level (1σ value) on a timescale of a few 100 seconds.

We have searched for periodic signals using standard techniques like the Phase Dispersion Minimization (PDM, Stellingwerf 1978) and the CLEAN algorithm (Roberts et al. 1987). The PDM periodograms obtained for the *Chandra* data, binned at either 100, 120 or 150 s, reveal a periodicity of 1500^{+100}_{-50} s. The obtained PDM statistic Θ is in the range 0.89–0.92. An *F*-test reveals that this periodicity could be the result of a random fluctuation with a probability of $\sim 40\%$ (see details in Stellingwerf 1978). This is not strange given the fact that the noise witihin individual PDM phase bins is two times higher than the overall detected variability. We note that simulations with even lower signal-to-noise ratios have revealed the good performance of PDM (as can be seen for the primary periodicity in Otazu et al. 2002, 2004). On the other hand, two additional possible periodicities of ~ 3050 and ~ 4600 s are detected with lower significance. Given their spectral profiles, it is clear that they are subharmonics of the ~ 1500 s periodicity (see Stellingwerf 1978 for details). The CLEAN

algorithm displays less significant maxima at ~ 1550 s, possibly because the signal is not perfectly sinusoidal but is better accounted for by a saw-tooth pattern with a slow increase and a relatively fast decay. However, sinusoidal fits to the binned data provide a possible period in the range 1545–1555 s, with a variability amplitude of 16%. We show in Fig. 14 the background subtracted *Chandra* lightcurve binned at 150 s intervals and normalized to its average value. We also present the same data smoothed with a running window of 450 s to enhance the 1500 s modulation, and a sinusoidal fit to the binned data, which approximately follows the relative maxima and minima of the smoothed data. In §6.5, we discuss these results, together with the light curves obtained using the *XMM-Newton* data (next section).

4. *XMM-NEWTON* RESULTS

4.1. *1WGA J1346.5−6255*

In order to fit the *XMM-Newton* spectrum of 1WGA J1346.5−6255, we attempted single component (thermal and non-thermal) and two-component models, as we did above for the *Chandra* data (§3.2). The *XMM* data allowed us however to extend the fits up to 8.5 keV. As with *Chandra*, we found that the power-law model provides an adequate fit with $N_H = 0.22 \pm 0.02 \times 10^{22}$ cm^{-2}, a photon index $\Gamma = 1.69^{+0.04}_{-0.05}$, and an unabsorbed X-ray flux of $2.22 \pm 0.02 \times 10^{-12}$ ergs cm^{-2} s^{-1} in the 0.5–8.5 keV energy range, with a reduced $\chi_\nu^2 = 1.04$ (for $\nu = 418$ degrees of freedom). As with the *Chandra* section, errors are at the 90% confidence level, unless otherwise mentioned. The spectrum is shown in Fig. 8, and the confidence contours for N_H and Γ are shown in Fig. 9.

By comparing the *XMM-Newton* to the *Chandra* parameters, we note that the *XMM*-derived N_H and Γ values are slightly higher than those derived from the *Chandra* analysis (§3.2). The contour plots however (Figs. 6 and 9) show that within errors, the values are consistent with each other, with the *XMM-Newton* values being much better constrained.

We subsequently tested for whether pile-up affected the *Chandra* spectral analysis (the *XMM-Newton* spectrum is not affected by pile-up). Using Webpimms and a count rate of ~ 0.10 counts s^{-1} in the 0.5–7.5 keV, we estimate a pile-up fraction of $\leq 12\%$ in ACIS-S3. We then corrected for pile-up using the *pileup* model in XSPEC. We find that the N_H and Γ values increase slightly and are closer to the best values obtained with *XMM-Newton*, but the range is still consistent with our previous *Chandra* estimates and the contour levels are very similar to those shown in Fig. 6. After correction for pile-up, we find that $N_H = 0.20^{+0.07}_{-0.09} \times 10^{22}$ cm^{-2}, and $\Gamma = 1.53^{+0.25}_{-0.33}$. The corresponding unabsorbed flux is $1.1^{+0.4}_{-0.2} \times 10^{-12}$ ergs cm^{-2} s^{-1}, consistent with the value before pile-up correction, but only accounting for ~ 50–55% of the flux detected by *XMM-Newton* in the 0.5–7.5 keV range. We conclude that while the spectral parameters are not significantly affected by pile-up, the difference in the flux estimate between the *Chandra* and *XMM* observations may be partly attributed to some contamination by the background and likely evidence for variability in the source (see §6 for a discussion on the variability of the source).

We then attempted pure MEKAL models. A onetemperature component MEKAL model provides a statistically acceptable fit, however the model overestimates the X-ray emission between 6–7 keV and is therefore discarded. Just like with the *Chandra* data, a two-temperature

MEKAL model provides a better fit with the following parameters: N_H= 0.16±0.01 ×10^{22} cm^{-2}, kT_1= 1.7±0.3 keV, kT_2= $13.0^{+2.6}_{-2.4}$ keV, χ^2_ν = 1.025 (ν=416 degrees of freedom). In Fig. 10, we show the EPIC spectra fitted with this two-component model and in Table 3, we summarize the results indicating that the harder component dominates the X-ray emission. In Fig. 11, we show the 68, 95 and 99.7% confidence contours for the fitted temperatures of the two-component MEKAL model. Note that the harder component's temperature is much better constrained with *XMM-Newton* than with *Chandra*. This temperature is still high for coronal emission but not inconsistent with the ones measured in the new γ Cas-like objects (see the discussion section).

Lastly, a two-component power-law+MEKAL model provides the best fit with the lowest χ^2_ν, with the following parameters: N_H = $0.21^{+0.03}_{-0.02} \times 10^{22}$ cm^{-2}, kT = $1.4^{+0.8}_{-0.3}$ keV, Γ = 1.60±0.07, reduced χ^2_ν=1.005 (ν=416 degrees of freedom). The corresponding fit is shown in Fig. 12 and the parameters summarized in Table 3. As in the MEKAL+MEKAL fit, the harder component (now the power-law) dominates the X-ray emission.

Finally, it is worth noting that the power-law fit (see Fig. 8) indicates that a bump near 6–7 keV is unaccounted for. Adding a Gaussian line to the power-law component improves the fit (χ^2_{415}=1.012), with an F-test probability of 0.117 that this improvement occurs by chance. The line energy parameters are: E_{line} = $6.77^{+0.14}_{-0.12}$ keV, σ_{line}=$0.19^{+0.13}_{-0.184}$ keV, and an unabsorbed line flux of 4.8 × 10^{-14} ergs cm^{-2} s^{-1}. Adding a Gaussian line near 6.7 keV to the two-component (MEKAL+MEKAL or MEKAL+power-law) models does not improve the fits significantly.

We conclude that the two-component MEKAL+MEKAL, power-law+MEKAL, and power-law+Gaussian line, all provide good fits to the *XMM-Newton* data, although the power-law+MEKAL provides the best fit, a result that is consistent with the *Chandra* study.

As for the *Chandra* data, we also obtained background subtracted lightcurves binned at 150 s and normalized to their average values. As can be seen in Fig. 15, 1WGA J1346.5−6255 was significantly variable, with an amplitude at the ±45–55% level (1σ values) on timescales of a few 100 seconds. A timing analysis reveals different possible signals at ∼4570, ∼8300 and ∼12000 s in the different lightcurves and using PDM or CLEAN. However, sinusoidal fits to the data with such periods do not converge. Since a marginal signal is nearly always detected at ∼1500 s with PDM and/or CLEAN, we have tried a sinusoidal fit around this periodicity, and found that convergence is achieved for a period of 1485±10 s and amplitudes of 10, 20 and 16% in the PN, MOS1 and MOS2 lightcurves (to be compared to the 16% amplitude in the *Chandra* data, §3.3). We have also analysed a combined data set of all normalized XMM data, and found similar results: the three possible periods reported above and a more clear signal than in individual data sets at 1486±2 s (and 2 subharmonics for PDM), with an amplitude of variability at the 13% level, hence closely matching the *Chandra* results. An *F*-test to the PDM results reveals a probability of up to 60% of this signal as being due to a random fluctuation. Although from the statistical point of view we can not argue that the periodicity exists, the detection of 2 subharmonics and the fact that we detect a very similar periodicity with *Chandra* and *XMM* data gives us confidence that the period, or quasi-period, is real. Future observations can probe this issue.

4.2. *G309.2–00.6*

We subsequently fitted the spectrum of the diffuse emission from the SNR G309.2−00.6. While a detailed study of the SNR is beyond the scope of this paper, we here present the spectral fit in order to compare its column density to that of 1WGA J1346.5−6255 (see Fig. 2), and therefore test for the association between the compact source and the SNR. Since G309.2−00.6 is believed to be a young SNR (Rakowski et al. 2001), we fitted its spectrum with a non-equilibrium ionization (NEI) model with variable abundances (*vnei* in XSPEC, Borkowski et al. 2001). A *vnei* model with solar abundances did not yield an acceptable fit (χ^2_ν = 10.5, ν = 169 degrees of freedom), a result that is consistent with the previous *ASCA* study by Rakowski et al. (2001). We subsequently varied the abundances of O, Ne, Mg, Si, S, Ar, Ca, Fe and Ni; and found that the model requires an over-solar abundance of Si and S, and an under-solar abundance of O, Ne, Mg, Ca and Fe. The plasma temperature is kT = 2.0±0.6 keV and the column density is N_H = $0.65^{+0.45}_{-0.25}$ ×10^{22} cm^{-2} (errors here are at the 3σ level, see Fig. 13). This best fit N_H value is at least three times higher than that derived for 1WGA J1346.5−6255 (see Tables 2 and 3). Even considering the upper 3σ value for 1WGA J1346.5−6255 with *Chandra* or *XMM* and the lower 3σ value for G309.2−00.6, N_H of the diffuse emission from the SNR is still higher. Therefore, based on the N_H values alone, we can conclude that 1WGA J1346.5−6255 is unlikely associated with the SNR. We note that this result does not agree with Rakowski et al.'s result, likely due to the lack of resolving power with *ASCA* which did not allow a study of the SNR independently of the 1WGA J1346.5−6255 point source.

5. OPTICAL RESULTS

The normalized classification spectrum of HD 119682 is shown in Fig. 16. It is covered in emission lines, most corresponding to Fe II transitions, and looks typical of Be stars. Spectral classification is complicated by the presence of many weak emission lines which render identification of weak absorption features very difficult. The spectral type can be estimated from the presence of both Si III and Si IV lines and a very weak He II 4686 Å line to be approximately B0.5. The determination of the luminosity class is complicated by the emission components and broadened lines, but the weakness of Si IV 4089 Å indicates that the star is not very luminous and suggests a luminosity class V. This is reinforced by the value of $\log g$ = 4.00 ± 0.10 dex found by Levenhagen & Leister (2004), which is consistent with the $\log g$ = 3.9 values for main sequence stars but clearly incompatible with the $\log g$ = 3.5 values for giants listed in Martins et al. (2005). Therefore, we will adopt a spectral classification of B0.5 Ve.

We note that the C III 4650 Å line is abnormally weak for a star of this spectral type, as it is always stronger than O II 4642 Å for any star earlier than B2. The N II 3995, 4041 Å lines are moderately stronger than expected, suggesting that there is a certain degree of CNO anomaly. This could explain the abnormal C III 4650 Å/O II 4642 Å ratio, as C could be moderately depleted and the λ 4642 Å line could have a contribution from N II 4640 Å.

The Equivalent Width of Hα emission line is −24 ± 2 Å. The shape is typical of a Be star with strong emission, and shows no discernible structure or asymmetry.

6. DISCUSSION

6.1. *Astrometry of HD 119682 and 1WGA J1346.5−6255*

The most precise position and proper motion of HD 11968 are given in Zacharias et al. (2004). Considering that our *Chandra* observations were conducted on year 2004.987, we obtain the following J2000 coordinates for that epoch: $\alpha = 13^{\rm h}\,46^{\rm m}\,32\fs579 \pm 0\fs005$, $\delta = -62°\,55'\,24\farcs17 \pm 0\farcs03$. This is perfectly consistent with the *Chandra* position of 1WGA J1346.5−6255: $\alpha = 13^{\rm h}\,46^{\rm m}\,32\fs6$, $\delta = -62°\,55'\,24''$ (with $1\farcs3$ error radius at 90% confidence level). However, given the high density of stars in the region where the X-ray source is located, we have estimated the chance coincidence probability of a 2MASS object (assuming negligible error in position, typically $\lesssim 0\farcs1$) falling within the *Chandra* error circle in position. We have done this by counting the 2MASS objects located within circles of different radius (1, 2, 3, 5, and $10'$) around the *Chandra* position, and found that the probability is always smaller than 4% for objects brighter than those present in the 2MASS catalog for this field: $J \simeq 18$, $H \simeq 17$, and $K_s \simeq 16$ mag. In fact, the absolute difference in position is just $0\farcs22$, much smaller than the $1\farcs3$ *Chandra* position error, providing a chance coincidence probability of $\simeq 0.1\%$, which practically confirms without any doubt the association between HD 11968 and 1WGA J1346.5−6255.

6.2. *Distances to HD 119682/1WGA J1346.5−6255 and SNR G309.2−00.6*

Our spectral type and luminosity class estimates of HD 119682 allow us to compute the distance to the star, and hence to 1WGA J1346.5−6255. For a B0.5 V star the absolute magnitude is $M_V = -3.6 \pm 0.4$ mag (slightly extrapolating from Martins et al. 2005) while the intrinsic color is $(B-V)_0 = -0.28 \pm 0.02$ (Johnson 1966). The average of the photometry in the literature, reported in §1, is $V = 7.97 \pm 0.06$ and $B-V = 0.16 \pm 0.05$ mag. The color excess is then $E_{B-V} = 0.44 \pm 0.07$ mag and the visual extinction is $A_V = 1.41 \pm 0.24$ mag (with $A_V = (3.30 + 0.28(B-V)_0 + 0.04 E_{B-V})E(B-V)$ from Schmidt-Kaler 1982). We finally derive a distance modulus of $V - M_V - A_V = 10.2 \pm 0.5$ and a distance to the source of $d = 1080 \pm 230$ pc.

However, HD 119682 is in fact a Be star, so the contribution from the stellar envelope to V and E_{B-V} should be considered. According to Dachs et al. (1988) and using our measure of the Hα Equivalent Width (*EW*) of -24 ± 2 Å, we should subtract a contribution from the envelope of $+0.05 \pm 0.02$ mag to E_{B-V} and -0.08 ± 0.02 mag to V, leading to star values of $V = 8.05 \pm 0.06$ and $E_{B-V} = 0.39 \pm 0.07$ mag. This provides a visual absorption of $A_V = 1.26 \pm 0.23$ mag, a distance modulus of $V - M_V - A_V = 10.4 \pm 0.5$, and a distance of $d = 1200 \pm 260$ pc. We note that our measure of the *EW* of Hα is not simultaneous to any of the used photometric data. However, since we use the average photometry, we expect these corrections to be approximately valid even if using a single value of *EW*. This distance estimate to HD 119682, of 1.2 ± 0.3 kpc, is in agreement, within errors, with the distance estimates to NGC 5281 reported in the literature, the average of which is 1.3 ± 0.3 kpc. Therefore, this will be the distance to HD 119682 adopted hereafter. We note that this is much lower than the distance estimates to SNR G309.2−00.6 appearing in the literature: 5.4 ± 1.6 kpc (Gaensler et al. 1998) and 4 ± 2 kpc (Rakowski et al. 2001).

Finally, by using $A_V = 1.26 \pm 0.23$ mag and the relationship of Predehl & Schmitt (1995) we obtain a hydrogen column density of $N_{\rm H} = (2.3 \pm 0.4) \times 10^{21}$ atoms cm^{-2}. This is perfectly consistent, within errors, with the values obtained from the X-ray spectral fitting of the *Chandra* and *XMM-Newton* data (see Figs. 6 and 9 and Tables 2 and 3). Therefore, there is no need for intrinsic absorption around the X-ray emitting zone.

We can now estimate the distances to the X-ray sources based on the measurements of the hydrogen column density, their conversion to extinction according to Predehl & Schmitt (1995) ($< N_{\rm H}/E_{B-V} > = 5.55 \times 10^{21}$ cm^{-2} mag^{-1}), and the value of the extinction per unit distance in the direction of the sources, which is of $E_{B-V}/d \sim 0.3$ mag kpc^{-1} (Lucke 1978). For this purpose we use the most accurate values of $N_{\rm H}$, obtained with the *XMM-Newton* data. For 1WGA J1346.5−6255 we consider the power-law model fit with $N_{\rm H} \sim (2.2 \pm 0.4) \times 10^{21}$ atoms cm^{-2} (3σ uncertainties) and obtain a distance of $d = 1.3 \pm 0.3$ kpc, fully consistent with the distance to HD 119682 and NGC 5281. (We note that the column density derived for the best fit power-law+MEKAL or power-law+Gaussian is close enough to that derived using the power-law and thus yields a similar distance estimate within error). For the diffuse emission of SNR G309.2−00.6 we use the *vnei* model fit with $N_{\rm H} = 6.5^{+4.5}_{-2.5} \times 10^{21}$ atoms cm^{-2} (3σ uncertainties) and obtain a distance of $d \lesssim 3.9^{+2.4}_{-1.5}$ kpc, consistent with the 4 ± 2 kpc value obtained by Rakowski et al. (2001) from their *ASCA* fit to the SNR. This distance is clearly incompatible with the distance to HD 119682/1WGA J1346.5−6255, but consistent within errors with the distance of 5.4 ± 1.6 kpc to the RCW 80 H II region proposed by Gaensler et al. (1998) to be associated with SNR G309.2−00.6.

6.3. *Circumstellar envelope*

The intrinsic $(J - K_s)_0$ infrared color of a normal B0,1 V star is −0.22 (Ruelas-Mayorga 1991). The 2MASS photometry provides a value of $J - K_s = 0.40 \pm 0.04$, leading to a total infrared color excess of $E_{J-K_s} = 0.62 \pm 0.04$. On the other hand, from the visual absorption of interstellar origin found above, $A_{V,\,\rm IS} = 1.26 \pm 0.23$ mag, and using the relationships by Rieke & Lebofsky (1985) we found interstellar infrared absorptions of $A_{J,\,\rm IS} = 0.36 \pm 0.06$ and $A_{K_s,\,\rm IS} = 0.14 \pm 0.03$, and finally $E_{J-K_s,\,\rm IS} = 0.22 \pm 0.07$. Therefore, in addition to the interstellar color excess, there is an extra contribution to E_{J-K_s} of 0.40 ± 0.08. This is typical of Be stars with strong emission lines, usually adscribed to their circumstellar envelope.

6.4. *Age of HD 119682*

Levenhagen & Leister (2004) report an age of 4 ± 1 Myr and a mass of $M = 18 \pm 1\,M_\odot$ for HD 119682 based on the evolutionary tracks by Schaller et al. (1992). In fact, according to the new evolutionary tracks by Meynet & Maeder (2003) (see their Fig. 5), the luminosity and effective temperature reported by Levenhagen & Leister (2004) are in agreement with a $18\,M_\odot$ star at the beginning of the main sequence or with a slightly evolved $20\,M_\odot$ star. However, since new calibrations such as the one of Martins et al. 2005 favor lower masses, we will consider as a strict upper limits for the age of HD 119682 the main sequence lifetime of a $15\,M_\odot$ star. On the other hand, since HD 119682 has a high rotational velocity of $v \sin i = 220 \pm 20$ km s^{-1}, we will use the evolutionary tracks by Meynet & Maeder (2003) for an initial rotational velocity of 300 km s^{-1}, leading to a total main sequence lifetime of 14.5 Myr (see their Table 1). Therefore, even if assuming the lowest possible mass and a high rotational velocity, the lifetime in the main sequence is less than 15 Myr,

i.e., 3 times lower than the estimated age of NGC 5281 by Sanner et al. (2001). This clearly confirms the blue straggler nature of HD 119682, which is not clear in the V vs. $(B-V)$ CMD of Sanner et al. (2001), slightly affected by the reddening of the envelope, but clearly evident when looking at the V vs. $(U-B)$ CMD of Moffat & Vogt (1973).

6.5. *On the nature of HD 119682/1WGA J1346.5−6255*

The unabsorbed X-ray luminosity of 1WGA J1346.5−6255 from our *Chandra* observations is $L_{(0.5-7.5 \text{ keV})} = 2.5^{+0.6}_{-0.7}(d/1.3 \text{ kpc})^2 \times 10^{32}$ ergs s^{-1} (using the range of fluxes tabulated in Table 2). From the *XMM-Newton* observations and using the range of fluxes obtained for the various models (Table 3), we obtain a luminosity of $L_{(0.5-8.5 \text{ keV})} = 4.5^{+0.1}_{-0.7}(d/1.3 \text{ kpc})^2 \times 10^{32}$ ergs s^{-1}, which corresponds to $L_{(0.5-7.5 \text{ keV})} = 4.1^{+0.2}_{-0.6}(d/1.3 \text{ kpc})^2 \times 10^{32}$ ergs s^{-1}, about a factor of 1.5–2 higher than the *Chandra* value, regardless of the model used. In any case, this is clearly lower than that of Be/X-ray binaries containing neutron stars, even the faint persistent ones (which have $L_X \sim 10^{34}$ ergs s^{-1}, see Reig & Roche 1999). Moreover, no X-ray pulsations have ever been detected, although Rakowski et al. (2001) could only constrain the pulsed fraction to be less than $\sim 85\%$ in the frequency range 0.002–32 Hz (0.03–500 s) at a 99.99% confidence level. Therefore, the currently available information does not favor the hypothesis of a binary system with an accreting neutron star as the compact object.

Another possibility would be to have a relatively quiescent accreting black hole in a binary system. Indeed, the photon index of 1WGA J1346.5−6255 is similar to those found in accreting black holes while in the low/hard state (see Fender et al. 2004 and references therein). Gallo et al. (2003) found a correlation between the 2–11 keV X-ray flux and the cm radio flux density for black holes in the low/hard state. >From our power-law model fit to the *XMM-Newton* data, we obtain an unabsorbed flux of $F_{2-11 \text{ keV}} = 1.7 \times 10^{-12}$ ergs cm^{-2} s^{-1} and compute an expected radio flux density of 0.29 ± 0.20 mJy at a distance of 1.3 kpc. Given the uncertainties, such a source could be above or below the 3σ level in the ATCA image of Gaensler et al. (1998). Deeper radio observations, with a noise smaller than 0.02 mJy, and with long baselines to avoid contamination from the SNR, would be needed to properly search for a radio counterpart. Only simultaneous X-ray observations could be useful to exclude the black hole scenario, although this would also be uncertain due to the scatter of the radio/X-ray correlation. However, we note that there is no clear evidence that a Be+black hole binary system has been found up to now. In addition, the X-ray spectra are better fitted including one or several MEKAL models, which is not the case for black holes in the low/hard state. Therefore, the scenario of an accreting black hole orbiting the Be star is not favored by the available data.

OB stars are known to be X-ray sources, presumably due to shocks arising in their stellar winds (see Güdel 2004 for a review). Based on *Einstein* data, Pallavicini et al. (1981) found that the X-ray luminosities of ~ 30 OB stars followed approximately the empirical law $L_X \simeq (1.4 \pm 0.3) \times 10^{-7} L_{\text{bol}}$. A more complete study based on *ROSAT* data for more than 200 OB stars allowed Berghöfer et al. (1997) to propose the existence of a correlation with two different power laws above and below $L_{\text{bol}} = 10^{38}$ ergs s^{-1}. The $\log L/L_\odot = 4.64 \pm 0.10$ value given by Levenhagen & Leister (2004) provides a star bolometric luminosity of $L_{\text{bol}} = (1.7 \pm 0.4) \times 10^{38}$ ergs s^{-1}, leading,

according to Berghöfer et al. (1997), to an X-ray luminosity of $L_X = (2^{+3}_{-1}) \times 10^{31}$ ergs s^{-1}. In contrast, the unabsorbed power-law X-ray luminosity from our *Chandra* observations, $L_{(0.5-7.5 \text{ keV})} = 2.5^{+0.6}_{-0.7}(d/1.3 \text{ kpc})^2 \times 10^{32}$ ergs s^{-1} is around one order of magnitude higher, while the *XMM-Newton* luminosity is even a factor of about 2 higher. In fact, the X-ray emission of HD 119682 is not only stronger than expected, but obviously harder than that of isolated stars: our *XMM-Newton* two-component MEKAL fit to the data requires a high temperature of $kT = 13.0^{+2.6}_{-2.4}$ keV ($14.3^{+2.9}_{-2.6} \times 10^7$ K), more than an order of magnitude higher than usual in main sequence B stars, and a factor of at least four higher than the most extreme cases (Cohen et al. 1997).

As a matter of fact, the luminosity and spectral shape of HD 119682/1WGA J1346.5−6255 are similar to those displayed by the notoriously peculiar Be star γ Cas: $L_{(2-10 \text{ keV})} = 6 \times 10^{32}$ ergs s^{-1} and two-component MEKAL spectrum with temperatures of 0.05 ± 0.01 keV and 12.3 ± 0.6 keV (Owens et al. 1999). Recently, Smith & Balona (2006) have proposed that the star HD 110432, which shows $L_{(2-10 \text{ keV})} \simeq 5 \times 10^{32}$ ergs s^{-1} and a MEKAL spectrum with $kT = 10.6 \pm 1.9$ kev (Torrejón & Orr 2001), is an almost perfect twin of γ Cas and have mentioned the possibility of the existence of a class of objects displaying similar characteristics, which they dub "γ Cas analogs". In addition, Motch et al. (2005) have very recently presented a summary of X-ray and optical properties of their proposed currently existing five "γ Cas-like objects" (plus γ Cas itself). The properties of HD 119682/1WGA J1346.5−6255, to be compared with their Table 1, are: spectral type B0.5 Ve, Hα EW of −24 Å, $L_{X (0.2-12 \text{ keV})} = 3.6–6.6 \times 10^{32}$ ergs s^{-1} (from the *Chandra* and *XMM-Newton* power-law model fits, respectively), $kT_{\text{soft}} = 1.7$ keV and $kT_{\text{hard}} = 13$ keV, and $\Gamma \sim 1.7$. These properties are practically identical to those of SS 397, with a slightly different equivalent width of Hα. Furthermore, one of the objects in the list of Motch et al. (2005) is a blue straggler in the 50 Myr old open cluster NGC 6649, closely matching the observed properties of HD 119682, also a blue straggler and located in the ~ 45 Myr old open cluster NGC 5281.

In the previous spectroscopic study, we showed that the X-ray flux of the 1WGA J1346.5−6255 source is a factor of ~ 2 brighter with the *XMM* observation than with the *Chandra* one, obtained 3 years later. This could be attributed to intrinsic variability of the source. The short-term variability detected on timescales of a few hundred seconds is similar to that seen in other γ Cas-like objects (Motch et al. 2005). Moreover, the periodicity of ~ 1500 s we have detected in HD 119682/1WGA J1346.5−6255, with a pulse fraction of 13–16%, is reminiscent to, although not so clear than, the oscillation found in the γ Cas analog HD 161103, with a period of 3250 ± 350 s and a pulse fraction of 24% (Lopes de Oliveira et al. 2006). However, in the case of HD 119682/1WGA J1346.5−6255, this possible period has been detected in two different observations performed with two different satellites, indicating that this signal is probably stable along time (although other superimposed signals are detected in the *XMM-Newton* data set).

In summary, HD 119682/1WGA J1346.5−6255 shares the following properties with the other γ Cas analogs: spectral fits including thermal components are better than simple power-law fits (see Tables 2 and 3); in the two-temperature MEKAL model fits, the cooler component is much fainter than the hard one (see Tables 2 and 3); the total photoelec-

tric absorption in X-rays is not very different from that due to the interstellar medium; the X-ray luminosity is in the range $L_{X\,(0.2\text{–}12\,\text{keV})} = 10^{32}\text{–}10^{33}$ ergs s^{-1}; there are no reported X-ray outbursts; the flux varies by a factor of a few from one observation to the other; variability on short timescales is detected, showing different quasi-periodic signals; the presence of an iron line near $\sim$6.7 keV (see §4.1 and Fig. 8), difficult to interpret in the black hole scenario; a moderate N enhancement; and a circumstellar envelope that contributes to the NIR reddening.

Therefore, we conclude that the overall properties of HD 119682 indicate that it is most likely a new γ Cas analog.

The nature of γ Cas analogs is still a matter of debate (see Motch et al. 2005 and Lopes de Oliveira et al. 2006 for recent discussions). Possible scenarios to explain the properties of the detected X-ray emission are the magnetic interaction between the star and its circumstellar decretion disk, or accretion on to a compact object (neutron star, white dwarf, or even a black hole). We note that the possible $\sim$1500 s period we have detected in HD 119682/1WGA J1346.5$-$6255 could be the rotational period in the neutron star or white dwarf scenario (although a long observation with *XMM-Newton* is needed to confirm it). In principle, optical spectroscopic observations of HD 119682 could unveil the presence of a compact object by means of a radial velocity curve, as has been done in the the case of γ Cas itself (Harmanec et al. 2000; Miroshnichenko et al. 2002). However, Be stars in X-ray binaries typically have orbital periods in the range $\sim$10–200 d, so a long-lasting observing program would be needed. In addition, the number and intensity of emission lines along the whole spectrum would render difficult to obtain accurate radial velocity measurements. Certainly, to obtain a radial velocity curve is not a straightforward task in the case of HD 119682.

Whatever the nature of HD 119682/1WGA J1346.5$-$6255, we stress that it is not related to the background SNR G309.2$-$00.6.

7. SUMMARY

After a study of the sources 1WGA J1346.5$-$6255 and SNR G309.2$-$00.6 with *Chandra* and *XMM-Newton* and of HD 119682 with the NTT, we have obtained the following results:

- The 1WGA J1346.5$-$6255 source is consistent with a point source. No jets have been observed with *Chandra*. We derive an upper limit on the unabsorbed flux from any unseen jets of 2.6×10^{-13} ergs cm^{-2} s^{-1} (0.5–7.5 keV), which corresponds to a luminosity of 5.3×10^{31} ergs s^{-1} at a distance of 1.3 kpc.

- The X-ray spectrum of 1WGA J1346.5$-$6255 is best fitted with two-component models including a thermal component. A two-component power-law+MEKAL model provides the best fits to the *Chandra* and *XMM* data. The hard component dominates the X-ray emission.

- The *Chandra* and *XMM*-derived N_H of $(1\text{–}3)\times10^{21}$ cm^{-2} (conservative range encompassing all models used) is lower than that towards the SNR: $(4\text{–}11)\times10^{21}$ cm^{-2} (3σ range).

- The *Chandra* flux of $\sim$ 1.0–1.5 $\times10^{-12}$ ergs cm^{-2} s^{-1} (0.5–7.5 keV, unabsorbed) is a factor of 1.5–2 lower

than that observed with *XMM-Newton*. Variability on short timescales (a few 100 seconds) has been also detected at a level of 45–55%, with a possible period of $\sim$1500 s in the *Chandra* and *XMM* data sets, which could be the rotational period of a neutron star or a whide dwarf.

- 1WGA J1346.5$-$6255 is coincident with the optical star HD 119682 whose spectrum is that of a B0.5 Ve star. It is a blue straggler in the $\sim$45 Myr old open cluster NGC 5281. The distance is 1.3$\pm$0.3 kpc, significantly lower than the distance to the SNR G309.2$-$00.6.

- Based on the above optical and X-ray spectral and timing properties of 1WGA J1346.5$-$6255, we conclude that it is unlikely to be a microquasar associated with the SNR G309.2$-$00.6, and that it is most likely a new member of the growing class of γ-Cas objects.

- Further X-ray observations are needed to study the variability of the source, and further explore the bump near 6.7 keV. Such a study will confirm the nature of 1WGA J1346.5$-$6255 as a γ-Cas like object.

- The search for a compact object associated with the G309.2$-$00.6 requires a deep *Chandra* observation of the SNR.

REFERENCES

Berghöfer, T. W., Schmitt, J. H. M. M., Danner, R., & Cassinelli, J. P. 1997, A&A, 322, 167

Borkowski, K. J., Lyerly, W. J., & Reynolds, S. P. 2001, ApJ, 548, 820

Cannon, A. J., & Pickering, E. C. 1918, Henry Draper Catalogue and Extension 1 (HD,HDE), Harv. Ann. 91–100 (1918–1924)

Cohen, D. H., Cassinelli, J. P., & Macfarlane, J. J. 1997, ApJ, 487, 867

Cutri, R. M., et al. 2003, VizieR Online Data Catalog, II/246 (http://cdsweb.u-strasbg.fr/viz-bin/Cat?II/246)

Dachs, J., Engels, D., & Kiehling, R. 1988, A&A, 194, 167

Draper, P. W., Taylor, M., & Allan, A. 2000, Starlink User Note 139.12, R.A.L.

Drilling, J. S. 1991, ApJS, 76, 1033

Dubner, G. M., Holdaway, M., Goss, W. M., & Mirabel, I. F. 1998, AJ, 116, 1842

Fender, R. P., Belloni, T., & Gallo, E. 2004, MNRAS, 355, 1105

Fitzgerald, M. P., Luiken, M., Maitzen, H. M., & Moffat, A. F. J. 1979, A&AS, 37, 345

Gaensler, B. M., Green, A. J., & Manchester, R. N. 1998, MNRAS, 299, 812

Gallo, E., Fender, R. P., & Pooley, G. G. 2003, MNRAS, 344, 60

Green, A. J. 1974, A&AS, 18, 267

Güdel, M. 2004, Astron. Astrophys. Review, 12, 71

Harmanec, P., et al. 2000, A&A, 364, L85

Høg, E., et al. 2000, A&A, 357, 367

Humphreys, R. M. 1975, A&AS, 19, 243

Jansen, F., et al. 2001, A&A, 365, L1

Johnson, H. L. 1966, ARA&A, 4, 193

Levenhagen, R. S., & Leister, N. V. 2004, AJ, 127, 1176

Lopes de Oliveira, R., Motch, C., Haberl, F., Negueruela, I., & Janot-Pacheco, E. 2006, A&A, 454, 265

Lucke, P. B. 1978, A&A, 64, 367

Martins, F., Schaerer, D., & Hillier, D. J. 2005, A&A, 436, 1049

Mermilliod, J.-C. 1982, A&A, 109, 37

Meynet, G., & Maeder, A. 2003, A&A, 404, 975

Miroshnichenko, A. S., Bjorkman, K. S., & Krugov, V. D. 2002, PASP, 114, 1226

Moffat, A. F. J., & Vogt, N. 1973, A&AS, 10, 135

Motch, C., Lopes de Oliveira, R., Negueruela, I., Haberl, F., Janot-Pacheco, E. 2006, in Active OB Stars: Laboratories for Stellar & Circumstellar Physics, eds. S. Stefl, S. P. Owocki & A. Okazaki. ASP Conf. Ser. 2006, in press, preprint (astro-ph/0512556)

Otazu, X., Ribó, M., Peracaula, M., Paredes, J. M., & Núñez, J. 2002, MNRAS, 333, 365

Otazu, X., Ribó, M., Paredes, J. M., Peracaula, M., & Núñez, J. 2004, MNRAS, 351, 215

Owens, A., Oosterbroek, T., Parmar, A. N., Schulz, R., Stüwe, J. A., & Haberl, F. 1999, A&A, 348, 170

Pallavicini, R., Golub, L., Rosner, R., Vaiana, G. S., Ayres, T., & Linsky, J. L. 1981, ApJ, 248, 279

Paredes, J. M. 2005, ChJAA, 5S, 121

Predehl, P., & Schmitt, J. H. M. M. 1995, A&A, 293, 889

Rakowski, C. E., Hughes, J. P, & Slane, P. 2001, ApJ, 548, 258

Reig, P., & Roche, P. 1999, MNRAS, 306, 100

Rieke, G. H., & Lebofsky, M. J. 1985, ApJ, 288, 618

Roberts, D. H., Lehár, J., & Dreher, J. W. 1987, AJ, 93, 968

Ruelas-Mayorga, R. A. 1991, Rev. Mex. Astron. Astrofis., 22, 27

Sanner, J., Brunzendorf, J., Will, J.-M., & Geffert, M. 2001, A&A, 369, 511

Schaller, G., Schaerer, D., Meynet, G., & Maeder, A. 1992, A&AS, 96, 269

Schmidt-Kaler, Th. 1982, Landolt-Börnstein: Numerical Data and Functional Relationships in Science and Technology, New Series "Group 6 Astronomy and Astrophysics", Volume 2

Shortridge, K., Meyerdicks, H., Currie, M., et al. 1997, Starlink User Note 86.15, R.A.L.

Skrutskie, M. F., et al. 2006, AJ, 131, 1163

Smith, M. A., & Balona, L. 2006, ApJ, 640, 491

Stellingwerf, R. F. 1978, ApJ, 224, 953

Stephenson, C. B, & Sanduleak, N. 1971, Publication of the Warner and Swasey Observatory, Cleveland, Ohio: Case Western Reserve University

Torrejón, J. M., & Orr, A. 2001, A&A, 377, 148

Townsley, L. K., Broos, P. S., Nousek, J. A., & Garmire, G. P. 2002, NIMPA, 486, 751, preprint (astro-ph/0111031)

White, N. E., Giommi, P., & Angelini, L. 1996, VizieR Online Data Catalog, IX/12 (http://cdsweb.u-strasbg.fr/viz-bin/Cat?IX/12)

Whiteoak, J. B. Z., & Green, A. J. 1996, A&AS, 118, 329

Zacharias, N., Urban, S. E., Zacharias, M. I., Wycoff, G. L., Hall, D. M., Monet, D. G., & Rafferty, T. J. 2004, AJ, 127, 3043
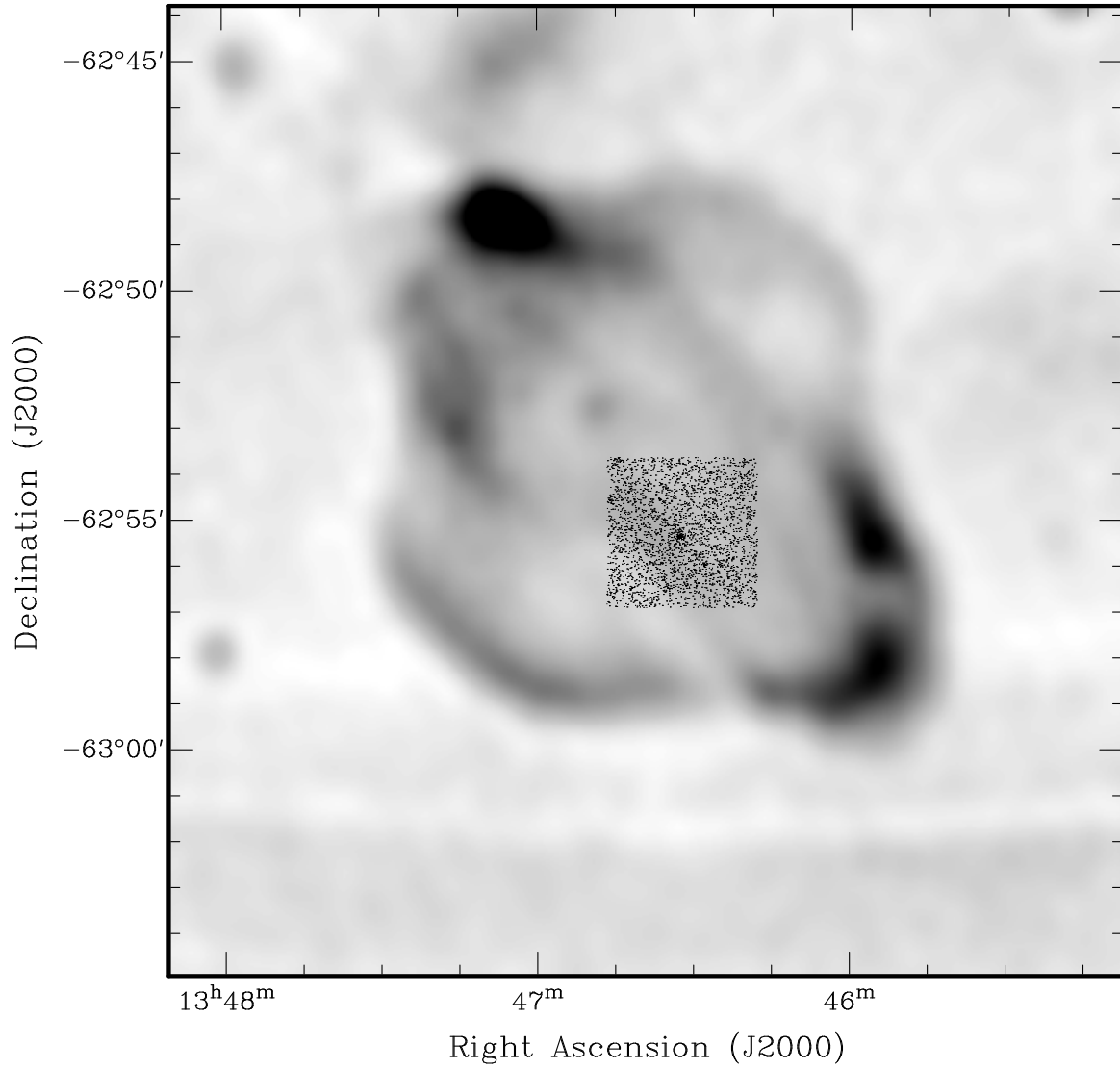
FIG. 1.— *Chandra* image (inset) overlayed on to a radio image of the supernova remnant G309.2–00.6, spanning $21' \times 21'$, obtained with MOST at 0.843 GHz, with a resolution of $43''$ (Whiteoak & Green 1996).
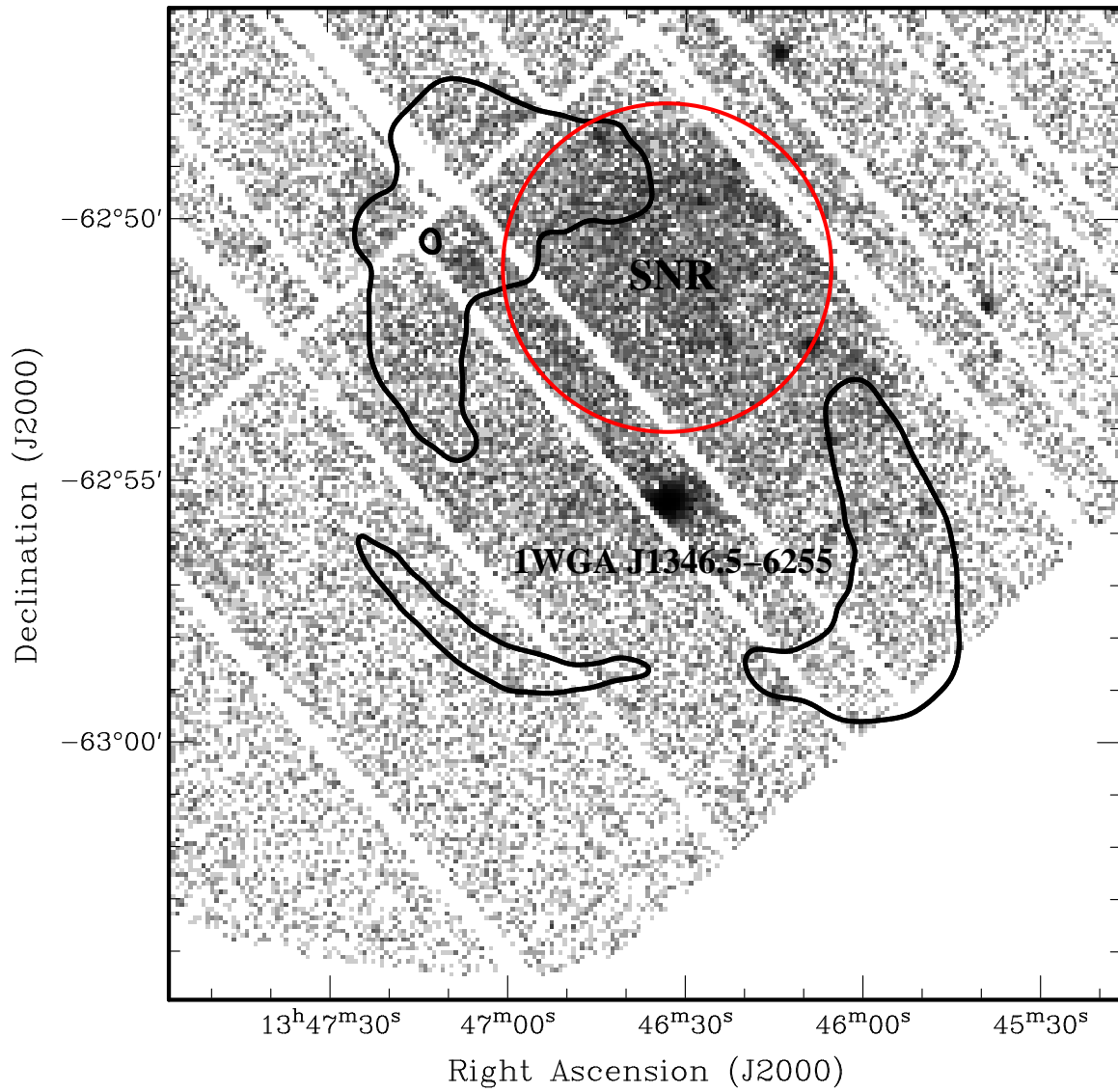
FIG. 2.— The *XMM-Newton*/PN image of 1WGA J1346.5−6255 and G309.2−00.6, spanning $20' \times 20'$, shown in logarithmic scale. The overlaid black contour corresponds to the brightest emission from G309.2–00.6 detected at 0.843 GHz with MOST. The overlaid circle denotes the region extracted from the *XMM* data for the spectral analysis of the diffuse emission from the SNR (see §4).
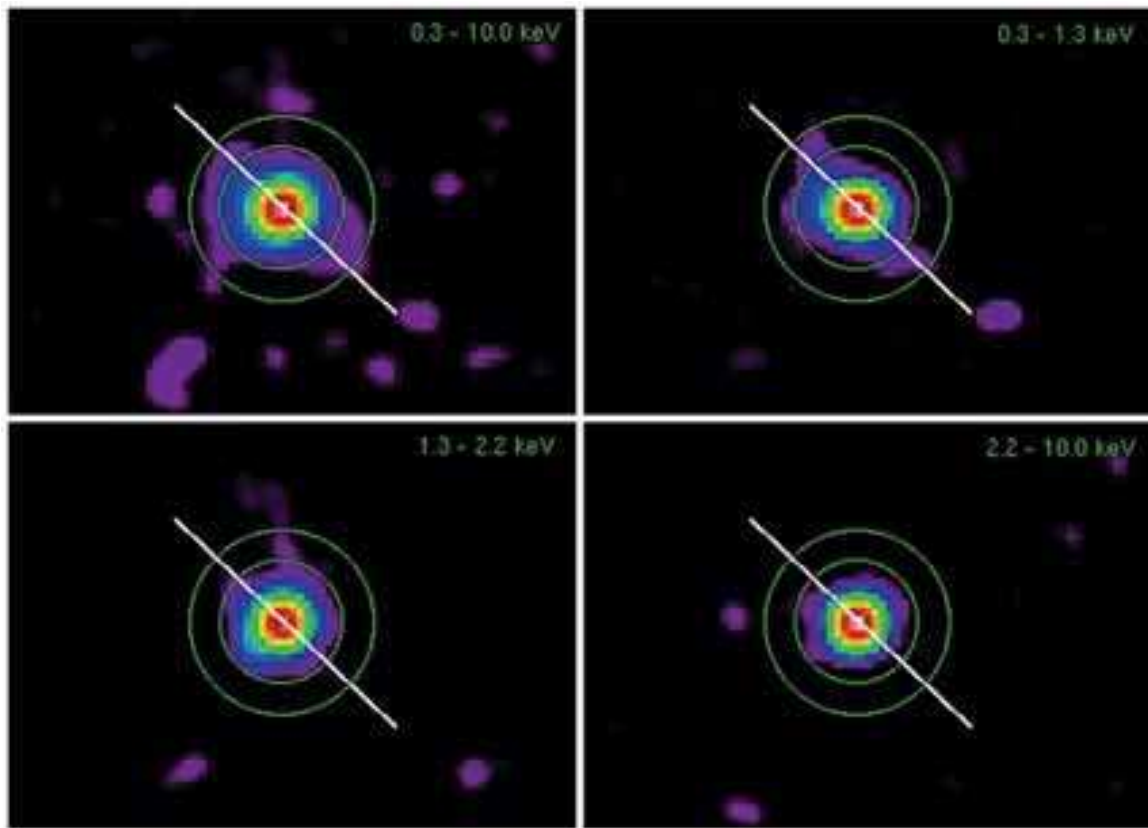
FIG. 3.— Top left: *Chandra* image of 1WGA J1346.5–6255 in the 0.3–10 keV energy range. The three other images correspond to the soft (top right), medium (bottom left) and hard (bottom right) energy ranges. The concentric circles have radii of 2 (barely visible), 4, and 6 arcseconds. The white line indicates the axis of symmetry of the G309.2–00.6 radio lobes. the images have been smoothed (minimum smoothing scale = 1 pixel, minimum signal-to-noise ratio = 2). There is a hint of extension in the soft energy band along the symmetry axis of the radio lobes, although the low count rate indicates that it is most likely background noise.
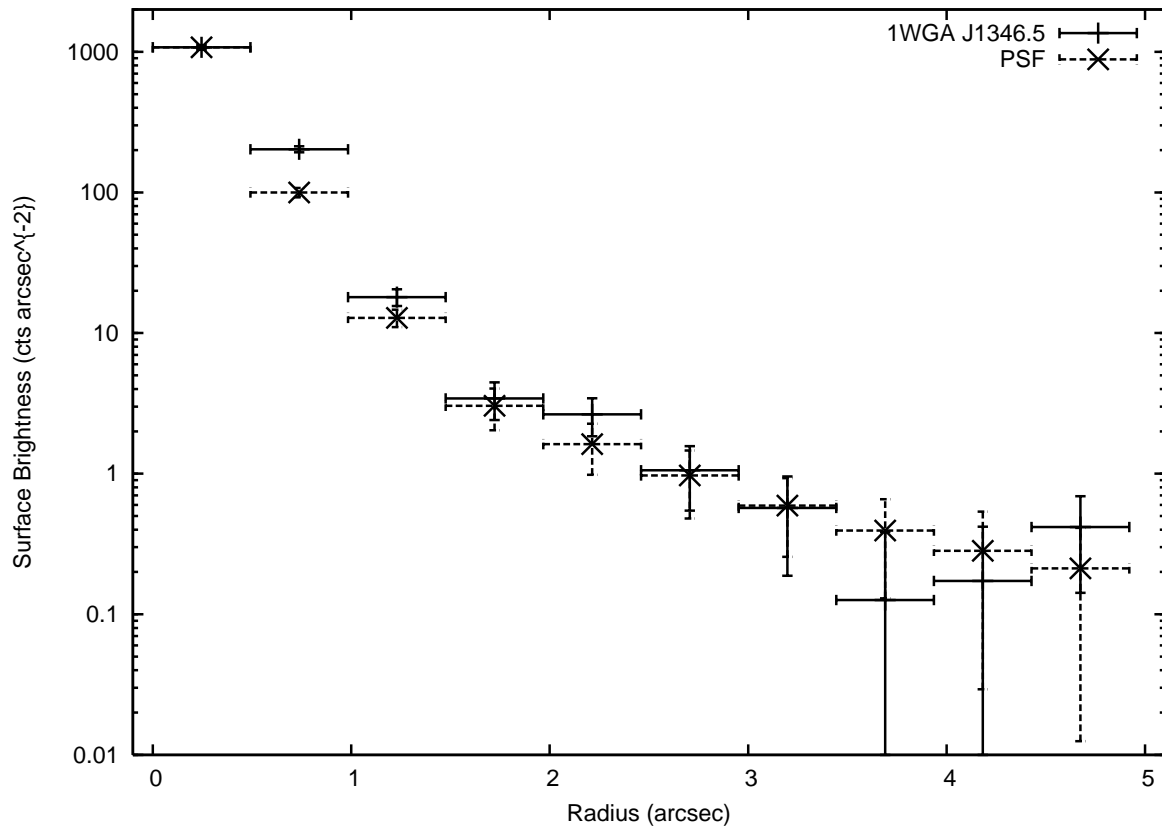
FIG. 4.— Radial profile of 1WGA J1346.5−6255 (solid bars with 90% confidence errors) and of *Chandra*'s PSF (dashed bars) in the 0.3–10.0 keV range (see §3.1 for details). The data are consistent with a point-like source.
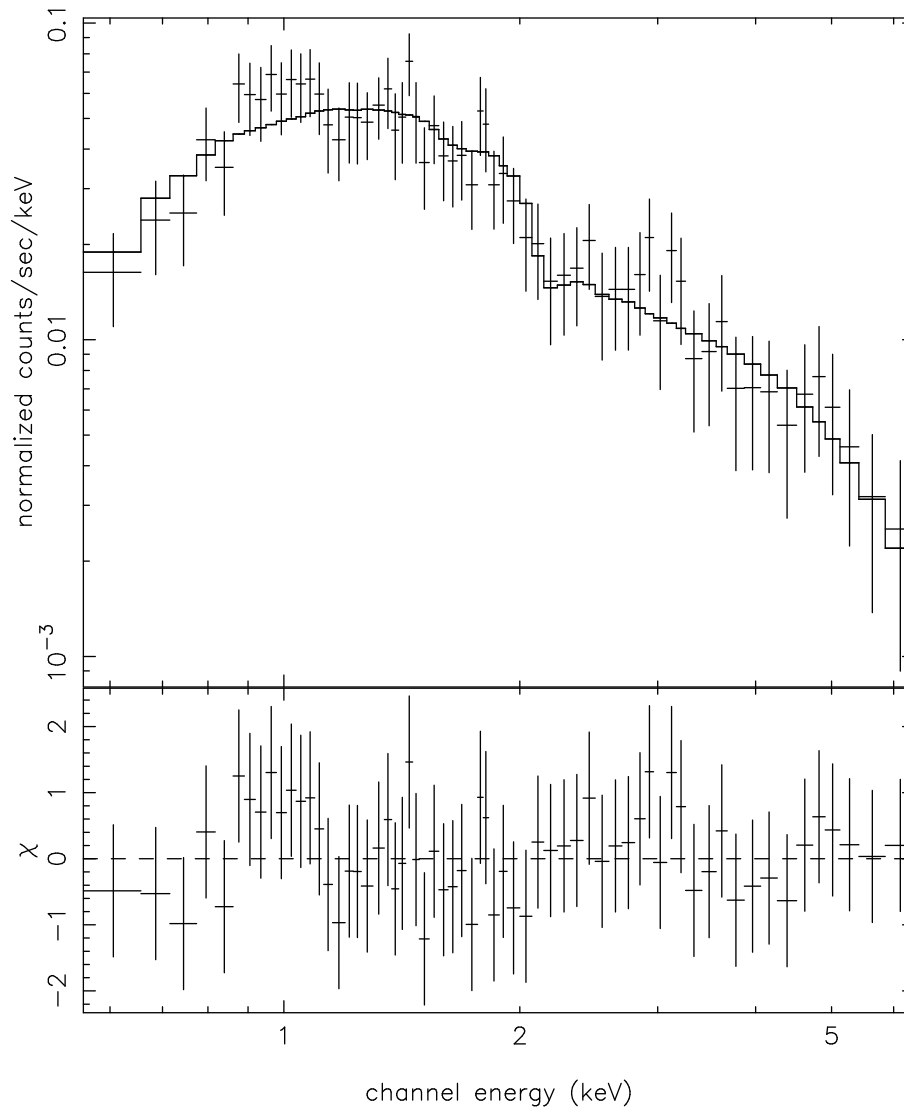
F<small>IG</small>. 5.— The *Chandra* spectrum of the point source 1WGA J1346.5−6255 fitted with an absorbed power-law model. The ratio of data to fitted model is shown in the bottom panel. An excess is seen around 1 keV.
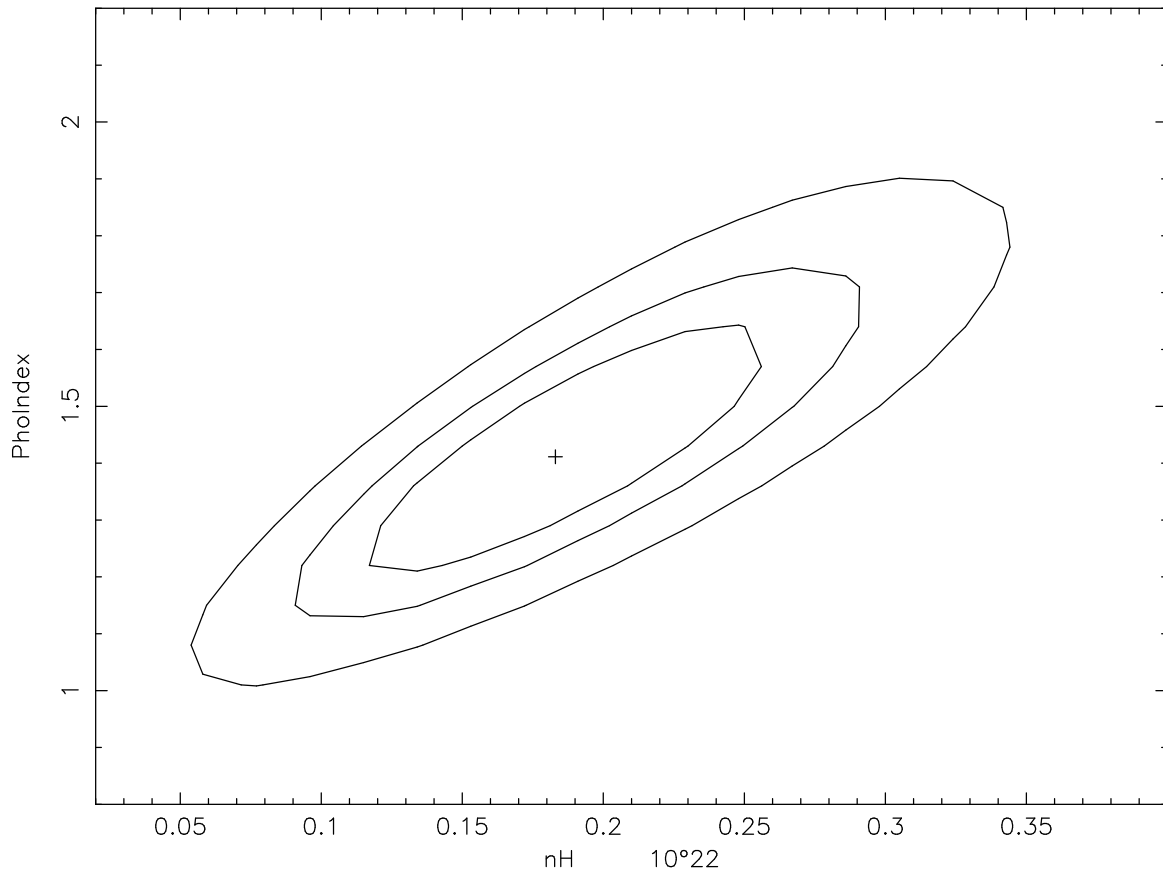
FIG. 6.— The 68, 95 and 99.7% confidence contours for the absorbed power-law model fit to the *Chandra* spectrum of 1WGA J1346.5−6255.
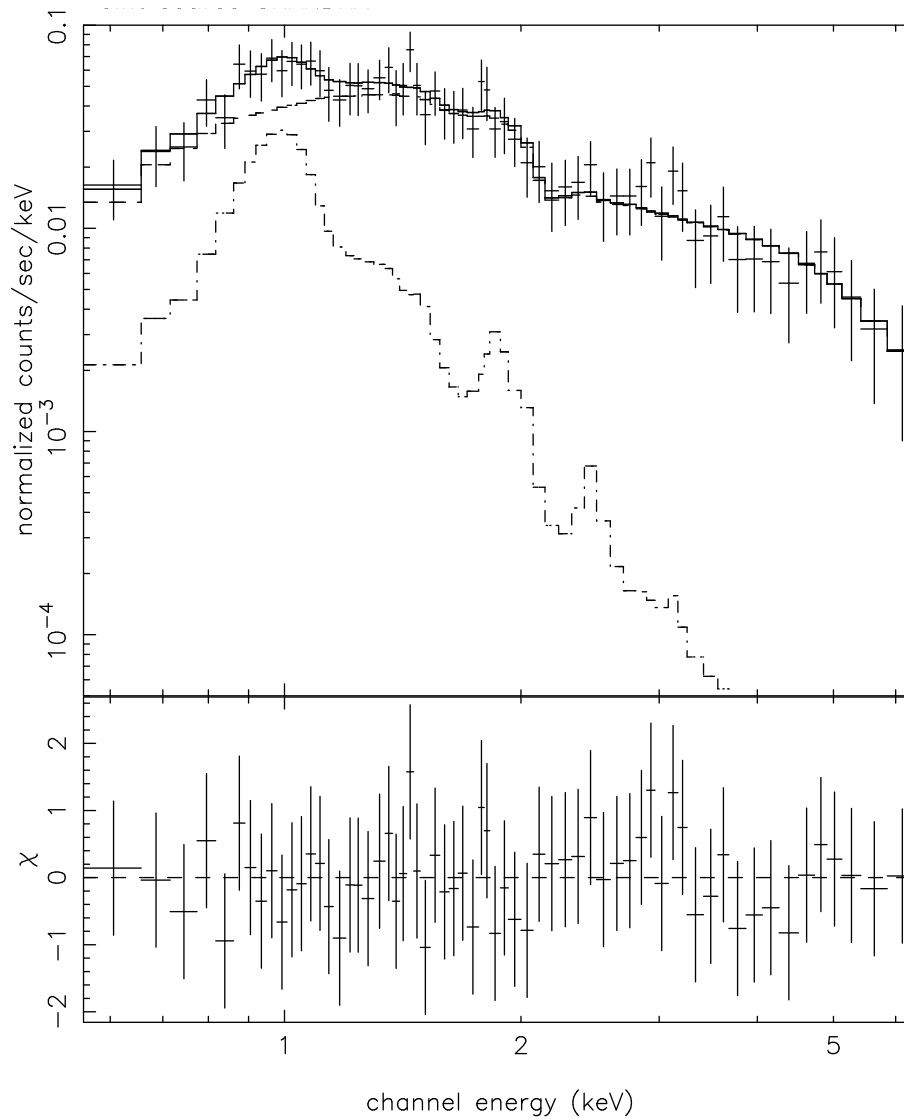
FIG. 7.— The *Chandra* spectrum of the point source 1WGA J1346.5−6255 fitted with an absorbed power-law+MEKAL model. The dot-dashed line represents the contribution from the MEKAL soft component, while the dashed line is for the harder power-law component. The ratio of data to fitted model is shown in the bottom panel.
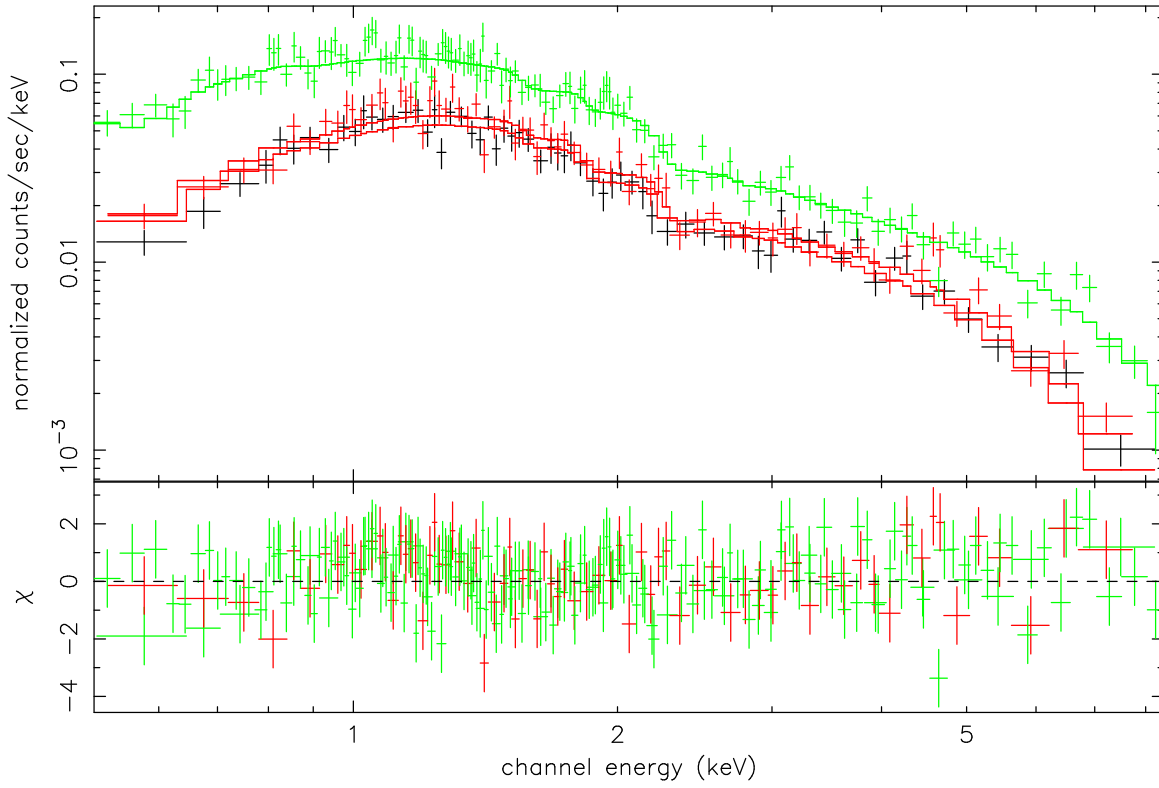
FIG. 8.— The *XMM-Newton* PN (green), MOS1 (black) and MOS2 (red) spectra of of the point source 1WGA J1346.5−6255 fitted with an absorbed power-law model. The bottom panel displays the ratio of data to fitted model.
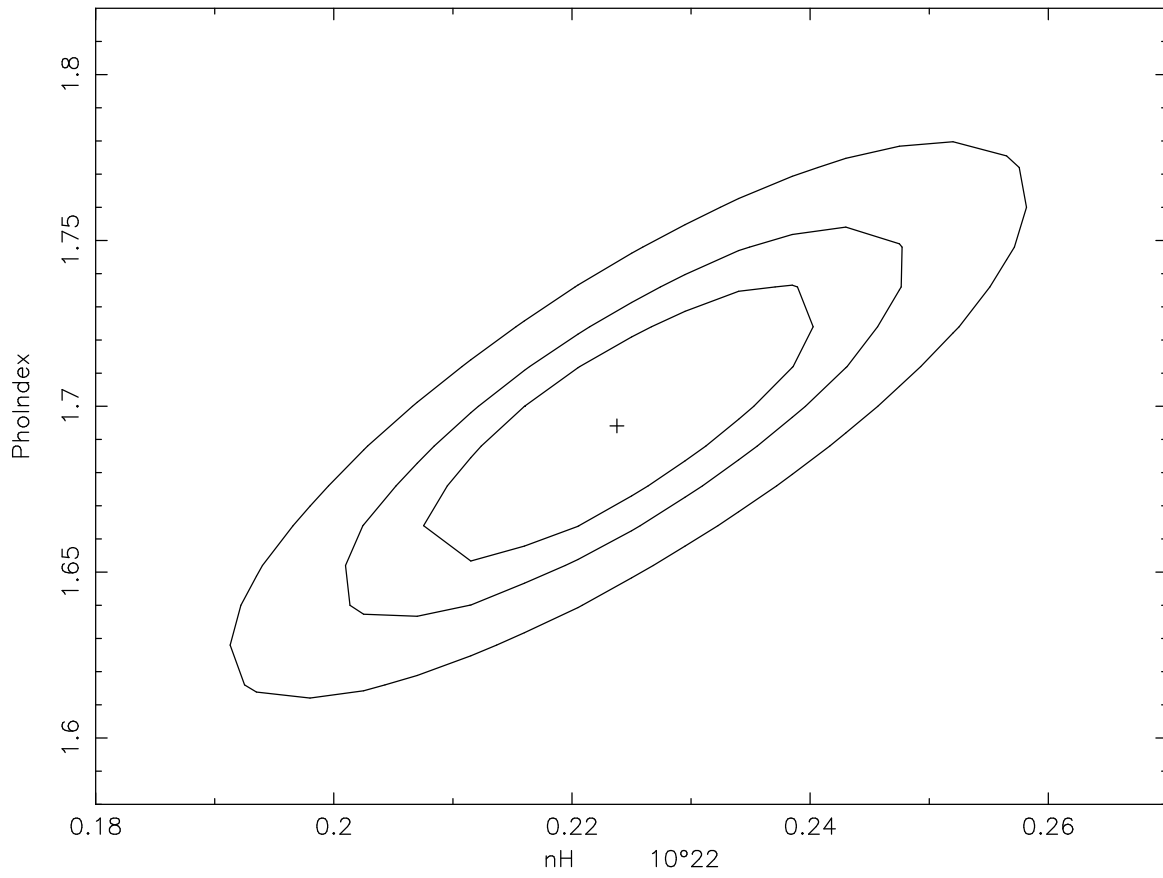
F<small>IG</small>. 9.— The 68, 95 and 99.7% confidence contours for the absorbed power-law model fit to the *XMM-Newton* PN and MOS spectra of 1WGA J1346.5−6255.
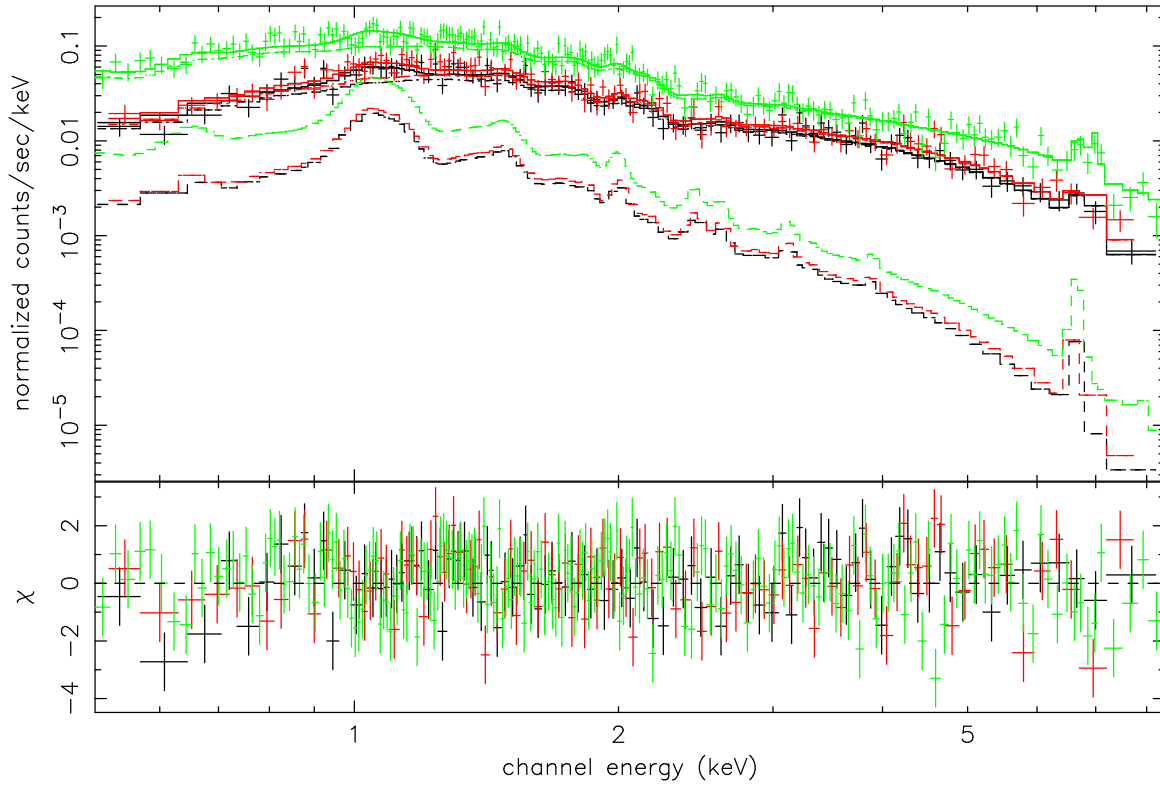
FIG. 10.— The *XMM-Newton* PN (green), MOS1 (black) and MOS2 (red) spectra of 1WGA J1346.5−6255 fitted with a two-component absorbed MEKAL model. The lower dashed lines indicate the contribution from the softer component (see text for details). The bottom panel displays the ratio of data to fitted model.
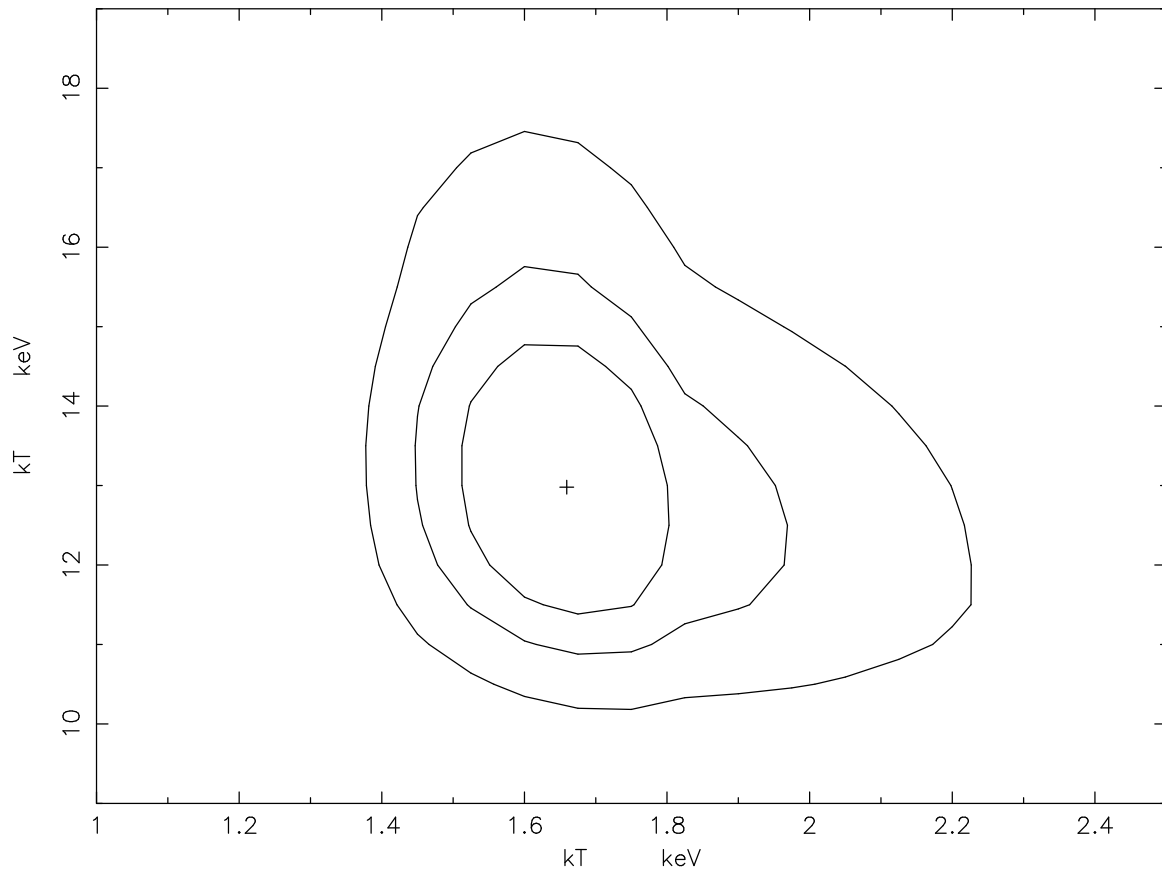
FIG. 11.— The 68, 95 and 99.7% confidence contours for the absorbed two-component MEKAL model fit to the *XMM-Newton* PN and MOS spectra of 1WGA J1346.5−6255.
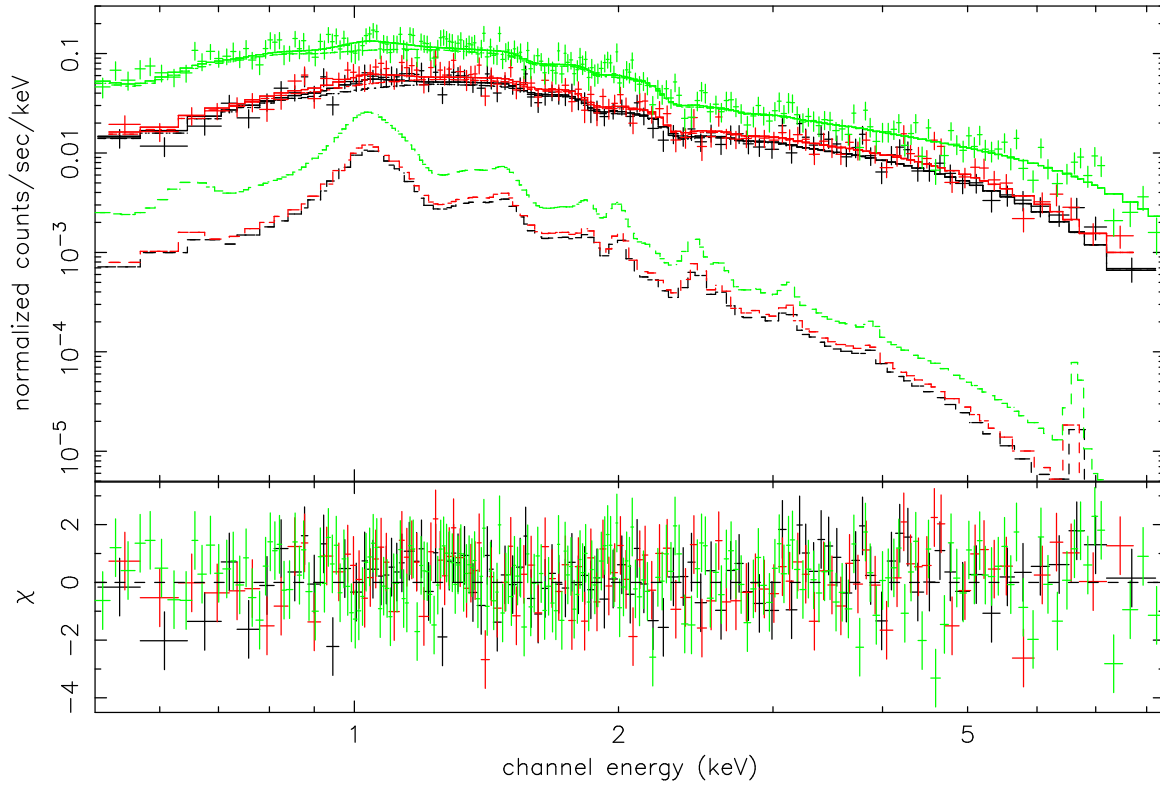
FIG. 12.— The *XMM-Newton* PN (green), MOS1 (black) and MOS2 (red) spectra of 1WGA J1346.5−6255 fitted with a two-component absorbed power-law+MEKAL model. The lower dashed lines indicate the contribution from the softer (MEKAL) component. The bottom panel displays the ratio of data to fitted model.
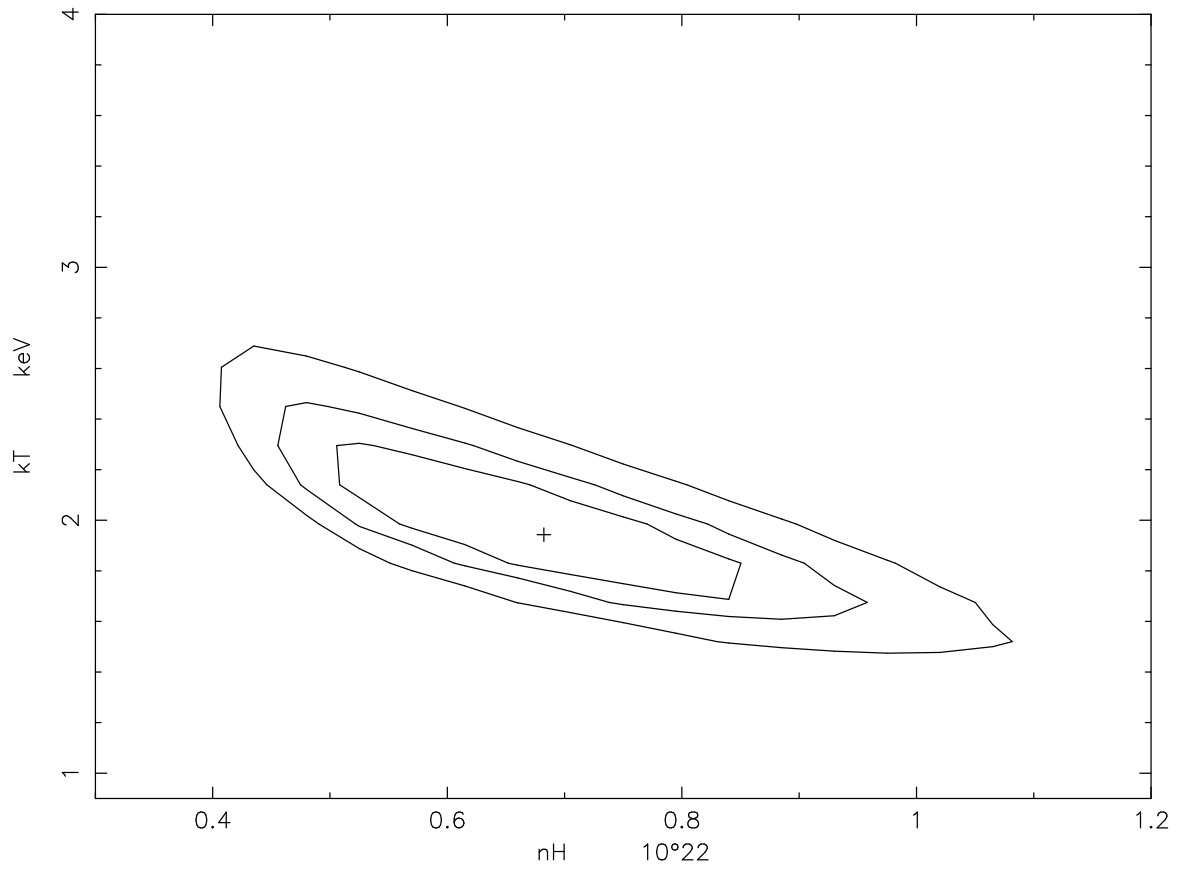
FIG. 13.— The 68, 95 and 99.7% confidence contours for the absorbed *vnei* model fit to the *XMM-Newton* PN spectrum of the diffuse emission from G309.2–00.6.
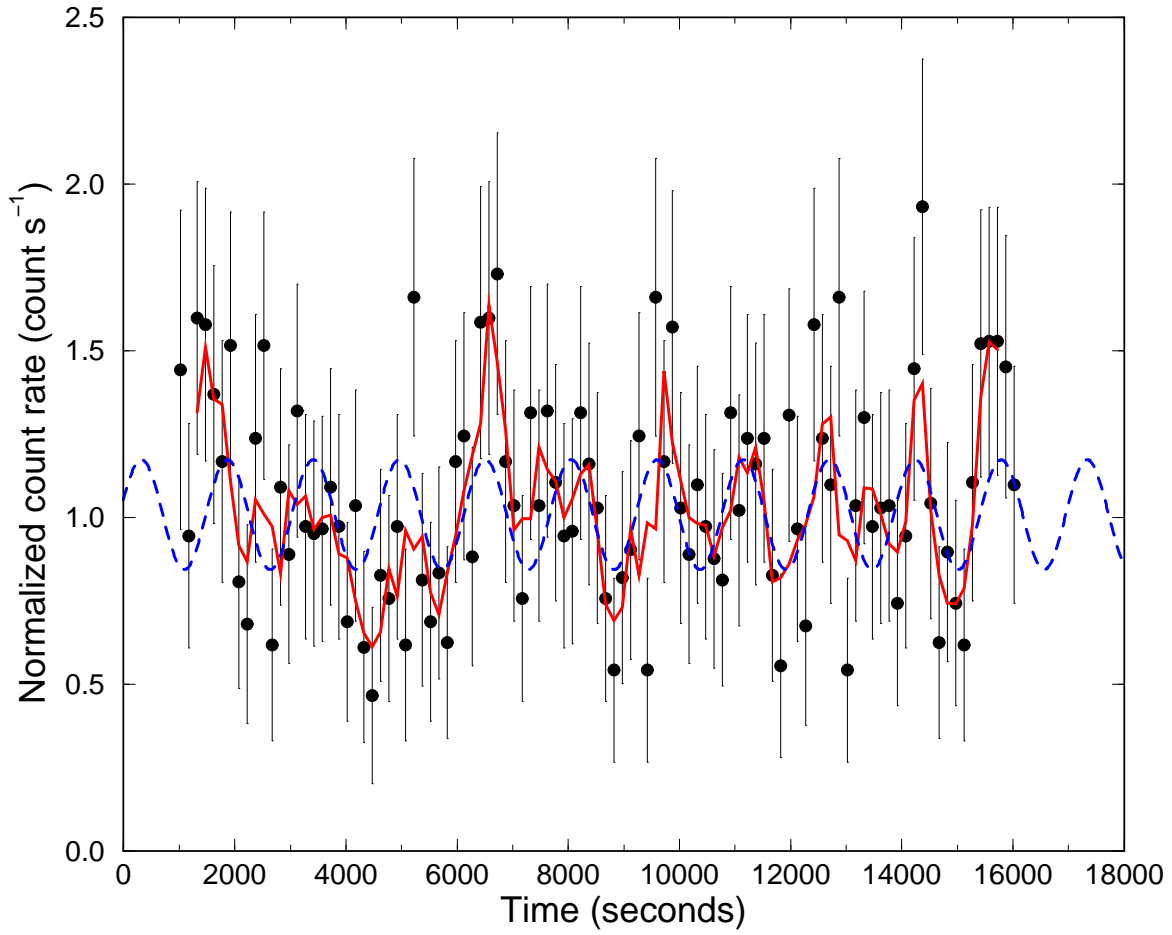
FIG. 14.— The normalized 1WGA J1346.5−6255 lightcurve obtained with *Chandra* after background subtraction and binning with 150 s (data points with 1σ error bars), smoothed with a running window of 450 s (solid line) and the sinusoidal fit to the binned data (dashed line). The time origin corresponds to 2004 December 26 at 09:22:20 UT (MJD 53365.3905). The data show significant variability and a quasi-periodic signal of ~1500 s.
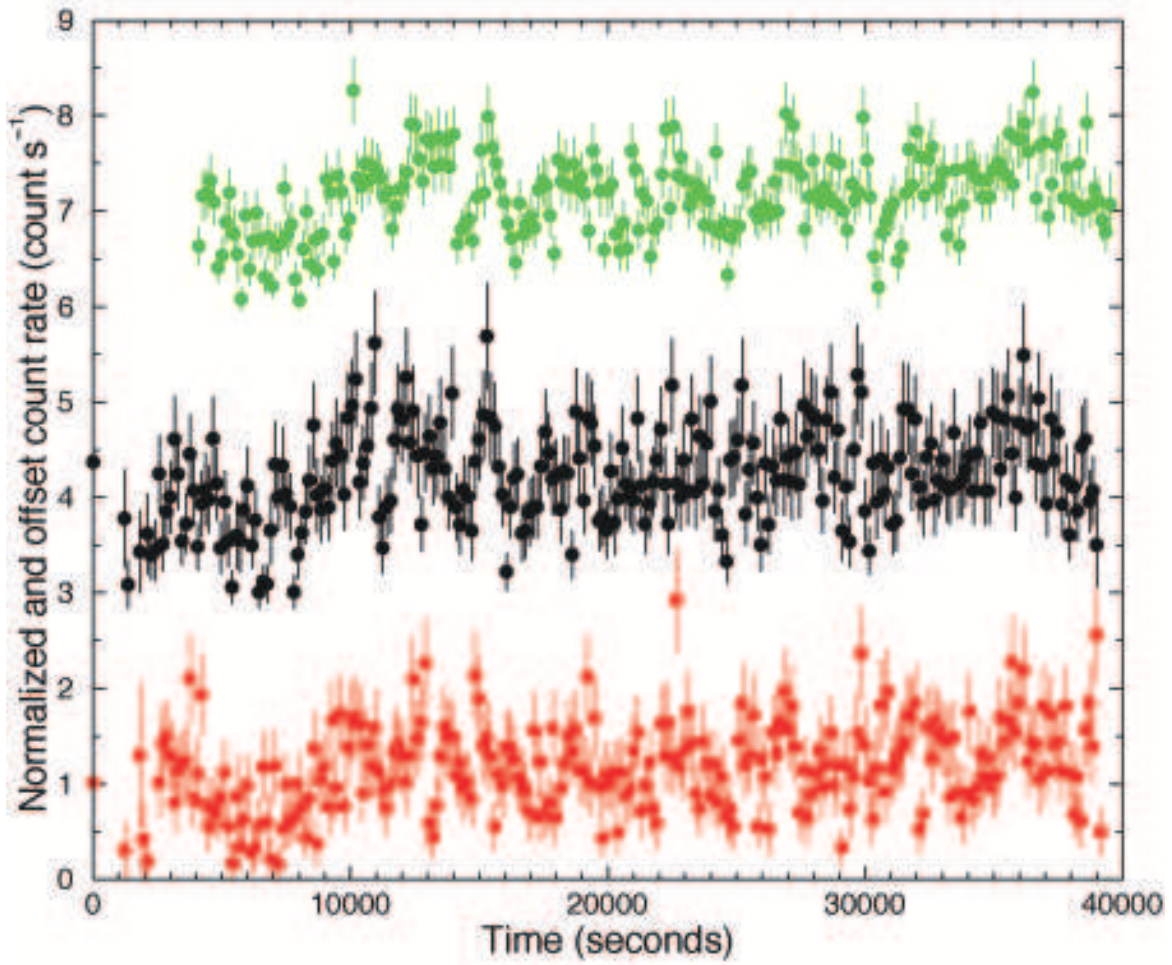
FIG. 15.— The normalized 1WGA J1346.5−6255 lightcurves obtained with *XMM-Newton* PN (top, green), MOS1 (middle, black), and MOS2 (bottom, red) data after background subtraction and binning with 150 seconds. Error bars are at the 1σ level. The time origin corresponds to 2001 August 28 at 02:52:50 UT (MJD 52149.1200). The data show significant variability with an amplitude at the 45–55% level with a timescale of a few 100 seconds (see §4.1 for details).
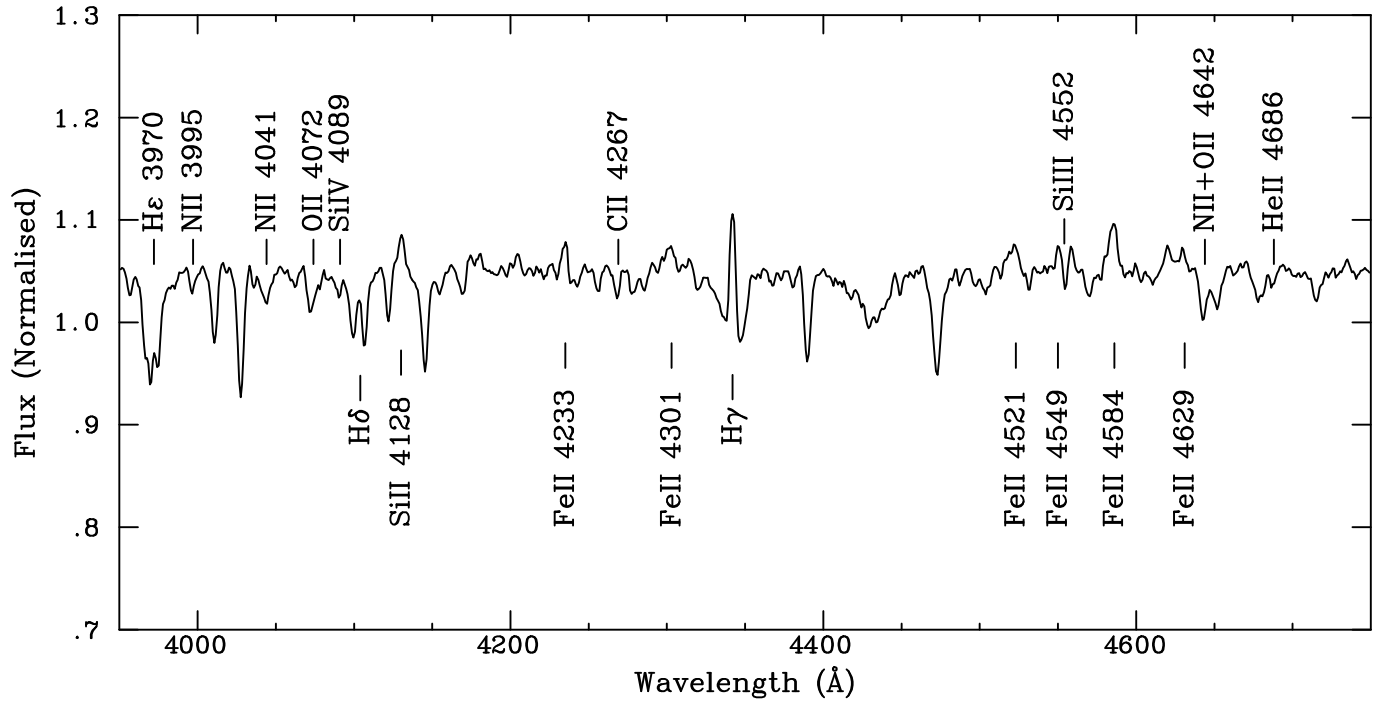
FIG. 16.— Classification spectrum of HD 119682, taken with EMMI on the NTT on 2003 June 5th. The most prominent emission lines and those absorption lines useful for classification purposes are labeled. For readability, none of the He I transitions typical of B-type spectra has been labeled. The C III 4650 Å line is not labeled either. Surprisingly, it is clearly weaker than the neighboring O II (+N II) 4642 Å line, suggesting a moderate N enhancement and C depletion. A classification of B0.5 Ve is inferred.

Safi-Harb et al.

TABLE 1
PHOTOMETRY OF HD 119682.

Ref.	V (mag)	$B-V$ (mag)
Moffat & Vogt (1973)	7.98 ± 0.01	0.13 ± 0.01
Humphreys (1975)	8.00	0.20
Drilling (1991)	8.06 ± 0.01	0.22 ± 0.01
Høg et al. (2000)	7.90 ± 0.01	0.08 ± 0.02
Sanner et al. (2001)	7.91 ± 0.04	0.16 ± 0.06
Weighted average	7.97 ± 0.06	0.16 ± 0.05

NOTE. — The Tycho-2 magnitudes (Høg et al. 2000) have been converted from VT and BT to V and $B-V$ magnitudes following their prescription. We have assumed an error of 0.05 mag for the Humphreys (1975) photometry to compute the weighted average. Errors are at the 1σ level.

TABLE 2
SPECTRAL FIT PARAMETERS OF 1WGA J1346.5−6255 OBTAINED
WITH *Chandra*.

Model	Parameters	Fitted values
wabs*power	$N_{\rm H}(\times 10^{22}$ cm^{-2})	0.18 (0.11–0.26)
	Γ	1.41 (1.19–1.65)
	norm ($\times 10^{-4}$)	1.58 (1.28–1.96)
	χ^2_ν (ν)	0.463 (61)
	flux ($\times 10^{-12}$ ergs cm^{-2} s^{-1})	1.13 (0.89–1.42)
wabs*mekal	$N_{\rm H}(\times 10^{22}$ cm^{-2})	0.15 (0.10–0.21)
	kT (keV)	26.9 (9.7–79.9)
	norm ($\times 10^{-4}$)	7.02 (5.92–9.16)
	χ^2_ν (ν)	0.480 (61)
	flux ($\times 10^{-12}$ ergs cm^{-2} s^{-1})	1.13 (0.94–1.23)
wabs*(mekal+mekal)	$N_{\rm H}(\times 10^{22}$ cm^{-2})	0.19 (0.12–0.28)
	kT_1 (keV)	0.95 (0.71–1.29)
	norm$_1$ ($\times 10^{-5}$)	3.10 (1.26–5.66)
	kT_2 (keV)	80 ($\geq$14)
	norm$_2$ ($\times 10^{-4}$)	8.2 (5.9–9.4)
	χ^2_ν (ν)	0.342 (59)
	flux ($\times 10^{-12}$ ergs cm^{-2} s^{-1})	1.16 (1.10–1.23)
wabs*(power+mekal)	$N_{\rm H}(\times 10^{22}$ cm^{-2})	0.19 (0.11–0.32)
	Γ	1.24 (0.98–1.52)
	norm$_\Gamma$ ($\times 10^{-4}$)	1.30 (0.98–1.53)
	kT (keV)	0.97 (0.69–1.34)
	norm$_{kT}$ ($\times 10^{-5}$)	3.38 (1.09–5.85)
	χ^2_ν (ν)	0.341 (59)
	flux ($\times 10^{-12}$ ergs cm^{-2} s^{-1})	1.18 (0.89–1.53)

NOTE. — All fits have been performed in the 0.5–7.5 keV energy range. The quoted fluxes are unabsorbed in the same energy range. The MEKAL models assume solar abundances. All confidence ranges are 90%.

TABLE 3
SPECTRAL FIT PARAMETERS OF 1WGA J1346.5−6255 OBTAINED WITH
XMM-Newton.

Model	Parameters	Fitted values
wabs*power	$N_H(\times10^{22}$ cm$^{-2})$	0.22 (0.20–0.24)
	Γ	1.69 (1.64–1.73)
	norm ($\times10^{-4}$)	3.77 (3.54–3.98)
	χ^2_ν (ν)	1.04 (418)
	flux ($\times10^{-12}$ ergs cm^{-2} s^{-1})	2.22 (2.20–2.24)
wabs*mekal	$N_H(\times10^{22}$ cm$^{-2})$	0.15 (0.14–0.16)
	kT (keV)	9.2 (8.5–10.8)
	norm ($\times10^{-3}$)	1.15 (1.11-1.19)
	χ^2_ν (ν)	1.12 (418)
	flux ($\times10^{-12}$ ergs cm^{-2} s^{-1})	2.15 (2.0–2.18)
wabs*(mekal+mekal)	$N_H(\times10^{22}$ cm$^{-2})$	0.16 (0.15–0.17)
	kT_1 (keV)	1.7 (1.4–2.0)
	norm$_1$ ($\times10^{-4}$)	1.07 (0.42–3.49)
	kT_2 (keV)	13.0 (10.6–15.6)
	norm$_2$ ($\times10^{-3}$)	1.08 (0.9–1.12)
	χ^2_ν (ν)	1.025 (416)
	flux ($\times10^{-12}$ ergs cm^{-2} s^{-1})	2.16 (2.15–2.17)
wabs*(power+mekal)	$N_H(\times10^{22}$ cm$^{-2})$	0.21 (0.19–0.24)
	Γ	1.60 (1.53–1.67)
	norm$_\Gamma$ ($\times10^{-4}$)	3.3 (1.6–3.0)
	kT (keV)	1.4 (1.1–2.2)
	norm$_{kT}$ ($\times10^{-5}$)	4.6 (2.5–16.8)
	χ^2_ν (ν)	1.005 (416)
	flux ($\times10^{-12}$ ergs cm^{-2} s^{-1})	2.20 (2.18–2.22)
wabs*(power+Gaussian)	$N_H(\times10^{22}$ cm$^{-2})$	0.23 (0.21–0.24)
	Γ	1.71 (1.66–1.76)
	norm ($\times10^{-4}$)	3.85 (3.63–3.97)
	E_{line} (keV)	6.77 (6.65–6.91)
	σ_{line} (keV)	0.19 (6×10^{-3}–0.32)
	norm$_{line}$ ($\times10^{-6}$)	4.33 (2.39–6.87)
	χ^2_ν (ν)	1.012 (415)
	flux ($\times10^{-12}$ ergs cm^{-2} s^{-1})	2.20 (1.88–2.26)

NOTE. — All fits have been performed in the 0.5–8.5 keV energy
range using PN, MOS1 and MOS2 data. The quoted fluxes are unab-
sorbed in the same energy range. The MEKAL models assume solar
abundances. All confidence ranges are 90%.